

1 **Ice-Nucleating Particles Near Two Major Dust Source Regions**

2
3 Charlotte M. Beall^{1,2}, Thomas C. J. Hill³, Paul J. DeMott³, Tobias Köneman^{2*}, Michael Pikridas⁴,
4 Frank Drewnick⁵, Hartwig Harder⁶, Christopher Pöhlker², Jos Lelieveld^{4,6}, Bettina Weber^{2**},
5 Minas Iakovides⁴, Roman Prokeš^{7,8}, Jean Sciare⁴, Meinrat O. Andreae^{1,2,9}, M. Dale Stokes¹,
6 Kimberly A. Prather^{1,10}

7 ¹Scripps Institution of Oceanography, University of California San Diego, La Jolla, CA 92037, USA

8 ²Max Planck Institute for Chemistry, Multiphase Chemistry and Biogeochemistry Departments, D-55128 Mainz,
9 Germany

10
11 ³Department of Atmospheric Science, Colorado State University, Fort Collins, CO 80523, USA

12
13 ⁴Climate & Atmosphere Research Center, The Cyprus Institute, Nicosia, CY-1645, Cyprus

14
15 ⁵ Max Planck Institute for Chemistry, Particle Chemistry Department, D-55128 Mainz, Germany

16
17 ⁶Max Planck Institute for Chemistry, Atmospheric Chemistry Department,
18 D-55128 Mainz, Germany

19
20 ⁷RECETOX, Faculty of Science, Masaryk University, Kotlarska 2, 611 Brno, Czech Republic

21
22 ⁸Department of Atmospheric Matter Fluxes and Long-range Transport, Global Change Research Institute of the Czech
23 Academy of Sciences, Belidla 4a, 60300, Brno, Czech Republic

24
25 ⁹Department of Geology and Geophysics, King Saud University, Riyadh, Saudi Arabia

26
27 ¹⁰Department of Chemistry and Biochemistry, University of California San Diego, La Jolla, CA, 92093 USA

28
29 *Now at Envicontrol GmbH, Waidmarkt 11, 50676 Köln, Germany

30
31 **Now at: Institute of Biology, University of Graz, 8010 Graz, Austria

32 Correspondence to: Charlotte M. Beall, cbeall@ucsd.edu

33 Abstract

34 Mineral dust and sea spray aerosol represent important sources of ice-nucleating particles (INPs), the minor
35 fraction of aerosol particles able to trigger cloud ice crystal formation and, consequently, influence multiple
36 climate-relevant cloud properties including lifetime, ~~reflectivity~~ radiative properties and precipitation
37 initiation efficiency. Mineral dust is considered the dominant INP source in many parts of the world due to
38 its ice nucleation efficiency and its sheer abundance, with global emission rates of up to 4700 Tg a⁻¹.
39 However, INPs emitted from the ocean surface in sea spray aerosol frequently dominate INP populations
40 in remote marine environments, including parts of the Southern Ocean where cloud-resolving model
41 simulations have demonstrated that cloud ~~reflectivity is~~ radiative properties are likely strongly controlled
42 by INPs. Here we report INP concentrations measured in aerosol and seawater samples during Air Quality
43 and Climate Change in the Arabian BASin (AQABA), a shipborne campaign that spanned the Red Sea,
44 Gulf of Aden, Arabian Sea, Arabian Gulf, and part of the Mediterranean. In aerosol samples collected
45 within a few hundred kilometers of the first and second ranked sources of dust globally, the Sahara and
46 Arabian Peninsula, INP concentrations ranged from 0.2 to 11 L⁻¹ at -20 °C with observed ice-active surface
47 nucleation-site densities (n_s) 1-3 orders of magnitude below levels predicted by mineral dust INP
48 parameterizations. Over half of the samples (at least 14 of 26) were collected during dust storms with
49 average dust mass concentrations between 150 and 490 $\mu\text{g m}^{-3}$ (PM₁₀), as simulated by the Modern-Era
50 Retrospective analysis for Research and Application, version 2 (MERRA-2). The impacts of heat and
51 peroxide treatments indicate that organics ~~were responsible for~~ dominated the observed ice nucleation (IN)
52 -activity at temperatures ≥ -15 °C with proteinaceous (heat-labile) INPs frequently observed at higher
53 freezing temperatures > -10 °C. INP concentrations in seawater samples ranged between 3 and 46 mL⁻¹ at
54 -19 °C, demonstrating the relatively low INP source potential of seawater in the region as compared to
55 seawater from multiple other regions reported previously. Overall, our results demonstrate that despite
56 proximity to the Sahara and the Arabian Peninsula and the dominance of mineral dust in the aerosol
57 sampled, existing mineral dust parameterizations alone would not skillfully represent the near-surface n_s in
58 the observed temperature regime (-6 to -25 °C). ~~The decreased n_s , and results demonstrating that organics~~
59 ~~dominated the observed IN activity > -15 °C, indicate that the IN active organic species are limited~~
60 ~~compared to the mineral IN components of dust.~~ Future efforts to develop or improve representations of
61 dust INPs at modest supercooling (≥ -15 °C) would benefit from a characterization of the specific organic
62 species associated with dust INPs. More generally, an improved understanding of the organic species
63 associated with increased IN -activity and their variability across dust source regions would directly inform
64 efforts to determine whether n_s -based parameterizations are appropriate for faithful representation of dust

Formatted: Font: (Default) Times New Roman

Formatted: Font: (Default) Times New Roman, 11 pt

Formatted: Font: 11 pt

Formatted: Font: (Default) Times New Roman, 11 pt

65 INPs in this sensitive temperature regime, whether region-specific parameterizations are required, or
66 whether an alternative to the n , approach is necessary. ▲

Formatted: Font color: Black

67 **1 Introduction**

68 Ice-nucleating particles (INPs) modulate the temperature and relative humidity at which ice
69 particle formation occurs in the atmosphere and thus are a key factor that controls ice-phase
70 partitioning in clouds. As initiators of ice formation and related phase-partitioning processes, INPs
71 affect multiple cloud properties and exert a strong influence on cloud lifetime, reflectivity-radiative
72 properties and precipitation initiation efficiency (e.g. Lohmann and Feichter, 2005; Vergara-
73 Temprado et al., 2018); (Brunner et al., 2021).

74 Globally, desert dust is likely the most abundant aerosol type by mass (Kinne et al., 2006; Kok et
75 al., 2021). Furthermore, multiple studies have demonstrated that mineral dust is the dominant ice-
76 nucleating (~~IN~~) species in many parts of the world based on observations (Ardon-Dryer and Levin,
77 2014; Boose et al., 2016; DeMott et al., 2015a; Price et al., 2018) and modeling of global INP
78 distributions (Burrows et al., 2013; Hoose et al., 2010; Murray et al., 2012; Vergara-Temprado et
79 al., 2017). Annual global dust emission rate estimates range between 400 and 4700 Tg a⁻¹ (Huneeus
80 et al., 2011; Kok et al., 2021). Of the average global dust loading in the atmosphere (20-29 Tg),
81 North African source regions are estimated to contribute ~50% (11-15 Tg), and the Middle East
82 and Central Asian source regions account for the bulk of the remainder, ~30% (7.7 Tg) (Kok et
83 al., 2021). Analysis of satellite products indicates that dust emissions rates are increasing over the
84 Middle East at a rate of 15% a⁻¹ (Klingmüller et al., 2016; Yu et al., 2018).

85 While Hoose and Möhler (2012) showed that mineral dust INPs generally activate ice crystals at
86 freezing temperatures < -15 °C, dust containing K-feldspar has been shown to nucleate ice at much
87 warmer temperatures, up to -4 °C (Atkinson et al., 2013; Harrison et al., 2016; Niedermeier et al.,
88 2015; Wex et al., 2014; Whale et al., 2015; Zolles et al., 2015). K-feldspars represent up to ~24%
89 of Saharan and Asian dusts by mass (Nickovic et al., 2012). However, knowledge of the abundance
90 and the available surface fraction of aerosolized K-feldspar would be necessary to evaluate the IN
91 efficiency of dust at temperatures > -15 °C (Kanji et al., 2017).

92 Though mineral dust is considered to be the dominant INP source in many regions, multiple
93 modeling and observational studies suggest that marine INPs are frequently dominant by number

94 in remote ocean regions in air masses with low concentrations of terrestrial aerosol (McCluskey et
95 al., 2018b, 2018c; Vergara-Temprado et al., 2017; Wilson et al., 2015; DeMott et al., 2016). Using
96 a global aerosol model to simulate marine organic and K-feldspar INP populations, Vergara-
97 Temprado et al. (2017) showed that the relative contribution of marine organic vs. dust INPs in
98 remote regions varies seasonally, and that marine organic INPs frequently outnumber K-feldspar
99 INPs (up to 100% of the simulated days in the Southern Ocean during summer). Results from a
100 follow-on cloud-resolving model study showed that Southern Ocean cloud reflectivity is strongly
101 modulated by INP concentrations, indicating that accurate estimates of the radiative energy budget
102 in the Southern Ocean likely require improved and reliable representation of both dust and marine
103 organic INPs (Vergara-Temprado et al., 2018). By generating isolated nascent sea spray aerosol
104 over a range of biological conditions, mesocosm studies have shown that marine INPs are
105 comprised of two classes: a dissolved organic carbon (DOC) type composed of IN-active
106 molecules and a particulate organic carbon (POC) type linked to the death phase of phytoplankton
107 blooms (McCluskey et al., 2017, 2018b).

108 Parameterizations for both marine and mineral dust populations are commonly implemented in
109 atmospheric models to estimate dust and marine INP concentrations. There are multiple existing
110 mineral dust INP parameterizations used to estimate their concentrations in aerosolized desert dust,
111 some based exclusively on laboratory measurements (e.g., Niemand et al., 2012; Ullrich et al.,
112 2017), and others derived from a combination of laboratory and field measurements (DeMott et
113 al., 2015). There are, additionally, multiple mineral-specific INP parameterizations including illite
114 (Broadley et al., 2012), kaolinite (Welti et al., 2012), quartz (Harrison et al., 2019) and K-feldspar
115 (Atkinson et al., 2013; [hereafter, "A13"](#)). The parameterizations by Ullrich et al. (2017; [hereafter,](#)
116 ["U17"](#)) and Niemand et al. (2012; [hereafter, "N12"](#)) were developed using dust samples from
117 multiple deserts, and both found little variability in the IN activity between dusts from locations
118 as disparate as the Sahara and Asia. DeMott et al. (2015; [hereafter, "D15"](#)) found agreement
119 between their observations-based parameterization and N12, supporting the validity of laboratory-
120 based parameterizations. Results in D15 also confirmed the conclusions of N12 and U17: that to
121 first order, dusts from distinct regions can be parameterized as a single particle type. The D15
122 parameterization has been considered to be representative of dust that has undergone atmospheric
123 photochemical and oxidative processes in transport (i.e., "aged" dust), because the

124 parameterization was derived from observations made far (1000s of kilometers) from the dust
125 emissions sources (Boose et al., 2016).

126 By contrast, few studies report *in situ* INP measurements near (e.g., < 1 day of transport) a major
127 dust source, and the lack of observations near dust source regions inhibit the evaluation of the
128 ability of existing dust INP parameterizations to represent nascent dust populations (Boose et al.,
129 2016; Gong et al., 2020; Price et al., 2018). INP observations are particularly lacking for the
130 sensitive temperature regime > -20 °C. Boose et al. (2016) found that D15 overpredicted INPs
131 observed during Saharan dust events at a location within 100s of km west of the Sahara (Izaña,
132 Tenerife, Spain) by 2-3 orders of magnitude, suggesting that aging may lead to increased IN
133 efficiency in mineral dust and that D15 may be less representative of nascent dust. These
134 conclusions were supported by Conen et al. (2015), who found that concentrations of INPs at -20
135 °C measured during Saharan dust events were one order of magnitude higher at Jungfraujoch in
136 the Swiss Alps than in Izaña, where dust events had occurred 1-7 d prior to reaching Jungfraujoch.
137 Gong et al. (2020) measured INPs in a variety of atmospheric and seawater sample types at Cabo
138 Verde and determined mineral dust to be the dominant source of INPs observed in the atmosphere
139 but found that INPs with freezing temperatures > -10 °C were likely biological. At altitudes
140 between 30 and 3500 m in the same region, Price et al. (2018) found that measured concentrations
141 of INPs ranged two orders of magnitude at a given temperature, and that the observed
142 concentrations related to the atmospheric dust loadings.

143 Recently, multiple studies have provided new, much-needed observations of ambient atmospheric
144 INPs in marine environments (DeMott et al., 2016; Hartmann et al., 2020; McCluskey et al., 2018c,
145 2018d; Yang et al., 2020) where data was historically lacking and, consequently, an impediment
146 to achieving predictive understanding of global INP distributions (Burrows et al., 2013). There
147 are now two parameterizations available for the estimation of atmospheric concentrations of
148 marine INPs emitted from the ocean surface: Wilson et al. (2015), which estimates cumulative
149 INPs from total organic carbon (TOC) concentrations in simulated sea spray aerosol (SSA), and
150 McCluskey et al. (2018), which estimates ice-active surface-nucleation-site density (n_s) from
151 aerosol surface area. Wilson et al. (2015) and McCluskey et al. (2018; hereafter “M18”) derived
152 marine INP parameterizations from field measurements of INPs in Atlantic and Arctic Ocean sea
153 surface microlayer samples and pristine SSA samples over the North Atlantic Ocean, respectively.

Formatted: Font: Italic

154 Here, we report observations of INPs measured in air masses influenced by both desert dust and
155 marine aerosol (Edtbauer et al., 2020) in close proximity to the two greatest global dust aerosol
156 sources: the Sahara (#1) and the Arabian Peninsula (#2) (Kok et al., 2021). INP concentrations
157 were measured in 26 ambient aerosol samples collected during Air Quality and Climate Change
158 in the Arabian Basin (AQABA), a shipborne campaign which took place July – August 2017 on a
159 transect that spanned the central and eastern parts of the Mediterranean, the Red Sea, the Gulf of
160 Aden, the Arabian Sea and the Arabian Gulf. The rest of this study will be structured as follows.
161 We present an overview of measurements and data sources in Sect. 2 Methods. In Results Sect.
162 3.1, an overview of INP concentrations observed is presented, followed by an assessment of
163 subsurface seawater (SSW) source potential (Sect. 3.2). ~~Observed~~Observed ~~ns~~ ~~were~~ ~~are~~ compared
164 to dust and marine INP parameterizations in Sect. 3.3, followed by an analysis of the, ~~and the~~
165 contributions of heat-labile (e.g., proteinaceous) and heat-stable organic compounds to observed
166 INP populations in aerosol (Sect. 3.4). The same analysis is applied to assess organic contributions
167 to observed INPs in a soil dust sample from a likely source region in Sect. 3.5. We discuss the
168 findings, potential INP sources and compare with prior studies in the Discussion Sect. 5. Finally,
169 in Sect. 5 we offer strategies to address the challenges of evaluating dust-specific INP
170 parameterizations and recommend measurements needed to develop predictive understanding of
171 dust INPs at modest supercooling ($T \geq 15^{\circ}\text{C}$). ~~were assessed via heat and peroxide treatments.~~
172 Finally, the potential INP source strengths of subsurface seawater (SSW) were assessed and
173 compared with SSW INP measurements from prior studies of remote and coastal seawater.

174 2 Methods

175 2.1 Project Overview

176 The AQABA campaign was conducted from 25 June to 3 September 2017 onboard the RV
177 *Kommandor Iona*. The research voyage was conducted in two transects: the first leg beginning in
178 La-Seyne-sur-Mer, France, heading through the Suez Canal, around the Arabian Peninsula and
179 ending in Kuwait, and second leg a return transect via the same route (Figs. S1-S2). The campaign
180 supported a large suite of on- and offline aerosol and gas-phase measurements (Bourtsoukidis et

181 al., 2019, 2020; Celik et al., 2020; Edtbauer et al., 2020; Eger et al., 2019; Friedrich et al., 2021;
182 Pfannerstill et al., 2019; Tadic et al., 2020; Wang et al., 2020).

183 2.2 Aerosol and Trace Gas Measurements

184 Aerosol size distributions were measured using an Optical Particle Spectrometer (OPC, Grimm
185 model 1.109) and a Fast Mobility Particle Spectrometer (FMPS, TSI model 3091). The OPC
186 measures particles in the size range 0.25 – 32 μm , and the FMPS measures particles with sizes
187 between 5.6 nm and 560 nm with 6s and 1s time resolution, respectively. The inlet for the aerosol
188 instrumentation was located at the top of a measurement container at a horizontal distance of about
189 1525 m from the INP filter sampling unit (Figs. S3-S4). To avoid condensation in inlet lines,
190 aerosol samples were passed through a drying system, which reduced ambient relative humidity
191 (RH) to an average value of $\approx 40\%$ in the measurement container. Ambient RH ranged between
192 67 and 81% during INP sampling periods. OPC and FMPS data were averaged over 1-minute time
193 intervals. A filter flag based on aerosol measurements was derived to identify and eliminate stack
194 emissions and applied to all aerosol data. The filter flag was based on short term variation in
195 particle number concentration measured by a Condensation Particle Counter (CPC, TSI model
196 3787), black carbon concentrations (Aethalometer, Magee AE33), wind direction and speed. The
197 flag was set when the apparent wind direction was from the direction of the stack ($\pm 30^\circ$) as seen
198 from the aerosol inlet position (Fig. S3) and strong fluctuations of black carbon and/or particle
199 number concentrations were observed relative to background levels. Two additional measurements
200 provided aerosol data from which a filter flag intended to identify and eliminate stack emissions
201 was derived: particle number concentrations as measured by a Condensation Particle Counter
202 (CPC, TSI model 3787) and black carbon concentrations (Aethalometer, Magee AE33). The filter
203 flag, based on short term variation in particle number concentration, black carbon concentration,
204 wind direction and speed, was applied to all aerosol data so that samples contaminated by stack
205 emissions could be identified. Particle losses were estimated using the Particle Loss Calculator
206 (von der Weiden et al., 2009). Losses were negligible ($<1\%$) up to 3.5 μm and increased to 40%
207 at 10 μm .

208 Particle surface area concentrations were derived from the 1-min time-averaged FMPS and OPC
209 measurements as follows. Geometric diameters were estimated from the measured mobility

Formatted: Font: Not Bold

Formatted: Font: Not Bold

Formatted: Font: Not Bold

Formatted: Font: Not Bold

Formatted: Font: Not Bold

Formatted: Font: Not Bold

Formatted: Font: Not Bold

Formatted: Font: Not Bold

210 diameters (FMPS) and optical particle diameters (OPC). Aerosols were assumed dry at sampling
211 conditions following the drying system described above. To convert optical particle diameters into
212 geometric diameters, it was assumed that all coarse particles ($d_p > 3000$ nm) were composed of
213 sea salt and dust with a mass ratio of 25% to 75%, and ~~for using~~ the respective refractive indices
214 and shapes the measured optical particle diameters were converted into geometric diameters (Sect.
215 S1.1). The sea salt:dust mass ratio was based on average dust and sea salt concentrations as
216 measured in particles < 10 μm (PM_{10} , see Sect. S2 for details).

217 Fine particle ($d_p < 700$ nm) sizes ~~were~~ was converted from optical diameter (d_{opt}) into geometric
218 diameter (d_{geo}) using the optical properties calculated from the PM_{10} -chemical composition of
219 particles < 1 μm (PM_1) as measured by an Aerosol Mass Spectrometer (Aerodyne HR-ToF-AMS),
220 assuming spherical particles (Celik et al., 2020). For particles in the intermediate size range (700
221 – 3000 nm), log-linear interpolation of optical and spherical properties was applied for conversion
222 of optical into geometric particle diameters (Sect. S1.2). The mobility diameters measured by the
223 FMPS were considered equivalent to the geometric diameter, assuming spherical particles. From
224 the resulting particle size distributions, particle surface area was calculated for each size bin. Total
225 particle surface concentrations were determined by integrating the surface area distribution for
226 particles up to 10 μm (d_{geo}). The overall uncertainty of derived particle surface area concentrations
227 is estimated to be 30%, including the uncertainty due to particle losses (see Sect. S3).

228 The water-soluble fraction of total suspended particles (TSPs) was monitored with hourly
229 resolution using a Monitor for AeRosols and Gases in Ambient Air, MARGA (Metrohm Applikon
230 model S2, Herisau, Switzerland). Sea salt concentrations were estimated by scaling measured
231 soluble Na^+ concentrations by 3.27 following Manders et al. (2009) and were used as a proxy for
232 SSA number concentrations. Size-resolved single particle chemical composition measurements
233 have shown that sea salt represents 50-70% of SSA particles by number ($d_p > 0.5\mu\text{m}$) (Collins et
234 al., 2014). Hourly composition data was linearly interpolated for 4 samples where 1-3 hours (of 7-
235 24 hours total sampling time) was missing (Fig. S53). The MARGA sampling line was
236 equipped with a PM_{10} cyclone, but the sample was not dried as the instrument is not prone to

Formatted: Font: Not Bold

Formatted: Font: Not Bold

Formatted: Font: Not Bold

Formatted: Font: Not Bold

Formatted: Font: Not Bold, Subscript

Formatted: Not Superscript/ Subscript

Formatted: Not Superscript/ Subscript

Formatted: Font: Not Bold

Formatted: Not Superscript/ Subscript

Formatted: Not Superscript/ Subscript

Formatted: Subscript

Formatted: Font: Not Bold

Formatted: Font: Not Bold, Subscript

Formatted: Font: Not Bold

Formatted: Font: Not Bold

237 ~~condensation. Particle transmission losses to the MARGA were estimated using the PLC and found~~
238 ~~to be consistent with the aerosol sizing instruments described above.~~

Formatted: Font: (Default) Times New Roman, 12 pt

239 Nitric oxide (NO) concentrations were measured using a commercially available two-channel
240 chemiluminescence monitor, CLD 790 SR (ECO Physics AG, Dürnten, Switzerland). During the
241 AQABA campaign, the CLD 790 SR, MARGA, FMPS, OPC, HR-ToF-AMS, CPC and
242 Aethalometer were operated within laboratory containers on the main deck of the research vessel.
243 The NO measurements were used to prevent stack sampling during INP collection (see Sect. 2.4).

244 **2.3 Dust Mass Concentrations from MERRA-2**

245 ~~Area-averaged. Since dust concentrations were not measured during the campaign, hourly dust~~
246 ~~surface mass concentrations along the cruise track were obtained from the (0.5 × 0.625 °)~~
247 ~~Modern-Era Retrospective analysis for Research and Application, version 2 (MERRA-2; Gelaro~~
248 ~~et al., 2017) and were averaged over the region covered during each sampling period. (Buchard et~~
249 ~~al., 2017) showed a high degree of correlation between MERRA-2 and surface dust concentration~~
250 ~~observations ($r \geq 0.69$), particularly during dust storms ($r \geq 0.92$). MERRA-2 surface dust mass~~
251 ~~concentrations also correlated well with PM_{10} observed during AQABA ($r \geq 0.71$) (Fig. S6).~~

Formatted: Subscript

252 MERRA-2 uses the GEOS-5 Earth system model (Molod et al., 2015; Rienecker et al., 2011) with
253 72 vertical layers between the surface and 0.01 hPa (~ 80 km) and the three-dimensional variational
254 data assimilation Gridpoint Statistical Interpolation analysis system (Kleist et al., 2009; Wu et al.,
255 2002, additional details in Sect. S4). ~~It simulates 5 types of aerosols (dust, sea salt, sulfate and~~
256 ~~black and organic carbon) using the Goddard Chemistry, Aerosol, Radiation, and Transport~~
257 ~~(GOCART) model (Chin et al., 2002; Colarco et al., 2010). Dust emissions and deposition rates in~~
258 ~~MERRA-2 are estimated by summing the emissions and deposition rates across GOCART~~
259 ~~simulated dust particles between 0.1–10 μm in size (dry diameter) (Gelaro et al., 2017). Dust~~
260 ~~emissions are constrained by wind-driven erosion over the source locations, which are identified~~
261 ~~from the topographic depression map (Ginoux et al., 2001). Aerosol observations are derived from~~
262 ~~various satellite products and are jointly assimilated within GEOS 5 with meteorological~~
263 ~~observations (Buchard et al., 2017). MERRA-2 has been shown to successfully reproduce the~~
264 ~~interannual variability of North Atlantic dust transport. Additionally, the improved aerosol~~

265 ~~assimilation scheme in MERRA-2 was shown to have a positive impact on the representation of~~
266 ~~long range dust transport from the Sahara compared to prior versions (Buchard et al., 2017).~~

267 **2.4 INP Measurements in Aerosol Measurement of Ice Nucleating Particles**

268 Ambient aerosol sampling for offline measurement of INPs was conducted from 5 Jul – 31 Aug
269 2017 on the *Kommandor Iona*'s wheelhouse top (platform above the bridge), ~125 m horizontally
270 from the online aerosol measurements inlet and ~135 m from the ocean surface (Figs. S3-4).
271 Sampling locations along the cruise transect corresponding to each aerosol sample are shown in
272 Figs. S1-2.

273 Aerosol samples were collected over 3-28 hour periods on polycarbonate filters (47 mm diameter,
274 0.2 µm pore-size, Whatman® Nuclepore, Chicago, Illinois, USA) placed in open-face Nalgene®
275 Analytical Filter Units (Waltham, Massachusetts, USA). Sampling intervals and frequency were
276 chosen with the aim of collecting > 5000 L during dust events and > 10,000 L when OPC particle
277 counts were relatively low (e.g., during sampling periods f040-44), as conditions allowed. Aerosol
278 sampling flow rates through the filter units were set to 10-13 ~~Lpm~~ LPM using a MassStream™
279 mass flow controller (Bethlehem, PA, USA) connected inline with a rotary vane pump (Thomas
280 QR-0100, Gardner Denver ©, Monroe, LA, USA). To decrease exposure to stack emissions, the
281 pump was automated to switch off when online measurements of NO exceeded one standard
282 deviation above the average background concentration for over 1 minute (~ 0.4 ± 0.8 ppb).
283 Comparing the stack contamination filter flag for aerosol measurements (Sect. 2.2) with INP
284 sampling periods additionally indicates no influence of stack emissions on INP filter samples.
285 Lacking a size-selective inlet for INP sampling, it is possible that aerosols > 10 µm were present
286 in INP samples during dust events. Surface area may be underestimated for these samples due to
287 the PM₁₀ cutoff for aerosol sizing (Sect. 2.2 and S3), but we do not expect this to affect our overall
288 conclusions as increased aerosol surface area would further reduce n_v , (see Results Sect. 3.3 and
289 Discussion Sect. 4).

290 Prior to sampling, filters were cleaned by soaking in 10 % peroxide (H₂O₂) for 10 minutes followed
291 by rinsing three times with deionized water, the last rinse further “polished” by passage through a
292 0.1 µm pore-size syringe filter (Puradisc, Whatman®, Maidstone, U.K). Filters were pre-loaded
293 into filter units in a laminar flow hood to further minimize contamination from handling. After

294 collection, each aerosol filter was placed in a 60 mm diameter sterile Petri dish (Life Science
295 Products, Frederick, Colorado, USA) using pre-cleaned acetyl plastic forceps (Fine Science Tools,
296 Foster City, California, USA), sealed with Parafilm and stored frozen (-20 °C). Samples were
297 shipped in a dry shipper via Cryoport® High Vol Shipper at -180 °C and upon arrival at the
298 laboratory were stored at -80 °C until processed, within 18 to 38 months ~~of~~ since collection. To
299 release collected particles, filters were immersed in 5-8 mL ultrapure water (Cat. Number W4502,
300 Sigma-Aldrich®, St. Louis, MO, USA) and shaken by hand for 20 minutes just prior to
301 measurement. ~~Eight samples were additionally diluted 100-fold to measure INP concentrations~~
302 ~~at lower freezing temperatures (Fig. S5).~~

303 INP concentrations were measured using the Scripps Institution of Oceanography SIO-Automated
304 Ice Spectrometer (SIO-AIS), an immersion freezing droplet assay instrument that is described in
305 detail in Beall et al. (2017). Briefly, the aerosol sample suspensions and SSW samples were
306 distributed in 30 ~~×~~ 50-μL aliquots into clean 96-well polypropylene sample trays (OPTIMUM®
307 ULTRA Brand, Life Science Products). An equal number and volume of aliquots of ultrapure
308 water accompanied each sample in the tray as a control. Trays were then inserted into an aluminum
309 block that was cooled at -0.87 °C min⁻¹ until the samples ~~are~~ frozen. Cumulative INP number
310 concentrations per temperature per volume liquid are calculated using the fraction (*f*) of unfrozen
311 wells per given temperature interval:

312

$$313 \quad n_{\text{INP,L}} = \frac{-\ln(f)}{V_d} \quad \text{Eq. (1)}$$

314

315 where V_d is the volume of the sample in each well (Vali, 1971). For aerosol filter samples,
316 cumulative INP number concentrations are calculated using the ratio of the ultrapure water volume
317 used for resuspension of the particles (V_{re}) to the volume of air sampled (V_A):

318

$$319 \quad n_{\text{INP}} = \frac{-\ln(f) \cdot V_{re}}{V_d \cdot V_A} \quad \text{Eq. (2)}$$

320

321 Prior to calculating n_{INP} , the fraction of unfrozen wells (f) was adjusted for contamination in the
 322 water used for suspension by subtracting the number of frozen ultrapure water wells per
 323 temperature interval from both the total number of unfrozen wells and total wells of the sample.
 324 The n_{INP} was additionally adjusted for background INPs from filters and sampling handling
 325 processes. Background ~~$n_{\text{INP_INP}}$ concentrations~~ were estimated using measured ~~$n_{\text{INP_INP}}$~~
 326 ~~concentrations~~ in aerosol sample field blanks, which had been ~~momentarily placed~~ placed in the
 327 sampling apparatus ~~~ 5s (without actuating the pump)~~ before removal and unloading and storage
 328 of the filter. Seven field blank samples were collected, one every ~ 7 days of the cruise (Fig. S7).
 329 INP concentrations were measured in field blanks as described above, and the n_{INP} simulated using
 330 the mean air volume sampled (6680 L). Figure S76 shows the estimated ~~n_{INP}~~ ~~n_{INP}~~ across the 7
 331 field blanks, which ranged between ~~$1.3.0 \times 10^{-4}$~~ and ~~$3.07.0 \times 10^{-32}$~~ L^{-1} at -20 °C. The freezing onset
 332 temperatures detected in the field blanks ranged between -6 and -27 °C. To correct ~~n_{INP}~~ ~~n_{INP}~~
 333 measured in aerosol samples for background INPs from sample handling, a linear regression ~~of~~
 334 ~~the average based on the geometric mean $n_{\text{INP_INP}}$ concentration~~ measured in field blank
 335 suspensions (mL^{-1} water) was used to estimate background concentrations of INPs in samples at
 336 all temperatures between -14.5 °C and -27 °C. The estimated background ~~$n_{\text{INP_INP}}$ concentration~~
 337 was then subtracted from the INP concentration measured in filter sample suspension volumes in
 338 this temperature range prior to calculating ~~n_{INP}~~ ~~n_{INP}~~ . The ~~n_{INP}~~ ~~n_{INP}~~ measured in one aerosol
 339 sample (f033) fell within the estimated INP background levels.

340 For this study, the detection limit was 0.68 ~~$n_{\text{INP_INPs}}$~~ mL^{-1} liquid or 0.001-0.0024 ~~$n_{\text{INP_INPs}}$~~ L^{-1}
 341 ~~air for the maximum and minimum~~ ~~and maximum~~ air volume sampled, respectively. To extend
 342 the upper limit of detection (i.e., the point at which all droplets have frozen) dilutions of 1:10 and
 343 1:100 were performed on 8 samples (Fig. S85).

344 The ice-active surface site density, n_s , is a metric used to define the ice-nucleating capabilities of
 345 an aerosol species (i.e., an aerosol sample of all the same particle type) (Kanji et al., 2017) as
 346 follows:

$$347 \quad n_s = \frac{N_{\text{ice}}}{N_{\text{tot}} \times A \text{ (cm}^2\text{)}} \quad \text{Eq. (3)}$$

348 where N_{ice} is the number of frozen droplets, N_{tot} is the total number of particles in a monodisperse
 349 aerosol population, and A is the surface area per particle.

350 The value of n_s can also be approximated for polydisperse aerosol samples containing multiple
351 aerosol types:

$$352 \quad n_s = \frac{N_{ice}}{A_{tot} (cm^2)} \quad \text{Eq. (4)}$$

353 where A_{tot} is the total surface area of the polydisperse aerosol ~~sample~~. The difference between the
354 n_s approximation (Eq. 4) and n_s (Eq. 3) is that many particle types are typically included in the n_s
355 approximation, and in an ambient aerosol measurement most of these are not ~~IN-active~~
356 ~~nucleating~~ (see also Hiranuma et al., (2015) Sect. 2.4). Furthermore, the subset of INPs in the
357 sample are likely also of different types, which likely have different n_s in the strict sense (Eq. 3).
358 Nevertheless, the n_s approximation is a useful metric for comparing the ice-nucleating ability of
359 different air masses and source regions and is often used for comparing data across studies of INPs
360 measured in ambient air. It is extremely challenging to separate measurements of INPs and surface
361 area by each particle type, and requires, for example, combining online measurements of single
362 particle chemistry, size distributions and INPs (Cornwell et al., 2019). All n_{INP} and n_s are reported
363 normalized to a standard temperature of 273.15 °K and pressure of 1013 hPa.

364 Heat and ~~hydrogen~~-peroxide-treatments were applied to a subset of samples (12 of 26) to test for
365 heat-labile biological (e.g., proteinaceous) and organic INP composition, respectively, ~~following~~
366 ~~the procedure described in~~ (McCluskey et al., (2018b) ~~and~~; Suski et al., (2018). ~~The 12 samples~~
367 ~~were selected based on sampling location with the aim of getting a representative measurement~~
368 ~~from each region~~. For each heat-treated sample, a 2 mL aliquot of the original ultrapure water
369 suspension was heated to 95 °C for 20 min in a water bath and re-tested ~~to assess the reduction in~~
370 ~~INP concentrations for changes in~~ n_{INP} . For peroxide treatments, 1.6 mL of the original suspension
371 was combined with 0.8 mL of 30% ~~H₂O₂-peroxide~~ (Sigma Aldrich®, St. Louis, Missouri, USA)
372 to achieve a final concentration of 10%, then the mixture was ~~immersed in water, and~~ heated to 95
373 °C for 20 min while being illuminated with two 26-W UVB fluorescent bulbs ~~to generate hydroxyl~~
374 ~~radicals~~. To remove residual ~~H₂O₂ peroxide and, to, prevent~~ otherwise significant freezing point
375 depression, the solution was cooled and catalase (Cat. Number IC10042910, MP Biomedicals,
376 Santa Ana, California, USA) was added. ~~Since catalase is itself decomposed by H₂O₂, while~~
377 ~~simultaneously catalyzing peroxide's disproportionation into water and oxygen, the enzyme was~~
378 ~~added in several 20-µL aliquots, allowing several minutes between each, until no effervescence~~
379 ~~resulted upon its addition~~. ~~Figure S7 shows the estimated n_{INP} in a heat and peroxide-treated blank~~

380 sample. Fisher's Exact Test was applied to frozen and unfrozen well fractions between each
381 untreated sample and its corresponding treated sample to test for significant differences ($p < 0.05$).
382 Note that significant difference in frozen well fraction is insufficient as a sole indicator of
383 sensitivity in peroxide treated samples because samples are diluted 2:3 (by 33%) compared to
384 untreated samples. ~~As n_{INP} INP concentrations~~ can be corrected for the dilution by scaling (as
385 opposed to frozen well fractions), the overlap in 95% binomial sampling confidence intervals
386 (Agresti and Coull, 1998) between the untreated and peroxide-treated sample is an additional
387 indicator of sensitivity for a given data point in the peroxide-treated sample spectrum within ± 0.2
388 °C, the uncertainty in the SIO-AIS temperature measurement (Beall et al., 2021). A lack of overlap
389 in the 95% binomial sampling confidence interval within ± 0.2 °C equates to a significance
390 threshold of $p < 0.005$ (Krzywinski and Altman, 2013).

391 INP concentrations were additionally measured in in untreated, heat-treated, and peroxide-treated
392 subsamples from an archived suspension of the soil dust sample N12 SD for comparison with this
393 study (DeMott et al., 2018; hereafter referred to as "N12-SD"). Briefly, the sample was generated
394 during the recent laboratory intercomparison of INP measurements (DeMott et al., (2018),
395 collected on a 0.2 μ m Nuclepore polycarbonate membrane filter (Whatman®, Chicago, Illinois,
396 USA) and stored frozen at -20 °C until processed, as described in DeMott et al (2018).

398 2.5 INP Measurements in SSW

399 INP concentrations were additionally measured in 10 SSW samples. For seawater sampling, a
400 water intake vertical steel pipe was positioned on the starboard of the ship approximately 2 m
401 below the sea surface level. The seawater was pumped into a 200 L stainless steel tank and
402 continuously exchanged at a rate of 3000 L h⁻¹. SSW samples for INP analysis were collected in
403 15 mL sterile centrifuge tubes (Falcon™, ThermoFisher Scientific, Waltham, Massachusetts,
404 USA) and stored frozen at -20 °C until they could be shipped in a dry shipper via Cryoport® (-180
405 °C) and ultimately stored at -80 °C as for aerosol samples until processed as described above (Sect.
406 2.4), within 18 to 38 months since collection. Storage duration was not correlated with INP
407 concentration changes in frozen marine and coastal precipitation samples (Beall et al., 2020). Heat
408 and ~~hydrogen~~ peroxide treatments as described above were applied to five-5 SSW samples from
409 the Arabian Sea and the Gulf of Aden. The focus on these regions was motivated by the detection

Formatted: Font: Bold

Formatted: Font: Bold

Formatted: Font: Bold

410 ~~of marine aerosol originating from the upwelling region in Somalia reported in~~ (Edtbauer et al.,
411 ~~(2020; see Sect. 3.3)~~, of these. To assess the contribution of submicron INPs to total measured
412 INPs, 2 mL of SSW was filtered through a 0.2 µm sterile syringe-filter (Acrodisc® Pall®, Port
413 Washington, New York, USA) and re-tested.

414 ~~INP concentrations in SSW collected at the Ellen Browning Scripps Memorial Pier at Scripps~~
415 ~~Institution of Oceanography (SIO; 32.8662 N, 117.2544 W) were assessed in 17 samples for~~
416 ~~comparison with SSW collected during AQABA. Samples were collected between 31 Jan and 7~~
417 ~~May 2016 in 15-30 mL sterile centrifuge tubes (Falcon™, ThermoFisher Scientific, Waltham,~~
418 ~~Massachusetts, USA) at depths of 1-3m and processed immediately using the SIO-AIS as~~
419 ~~described above.~~

420 ~~2.5 FLEXPART Back Trajectories~~

421 ~~Air mass 72-hour back trajectories for each sample were simulated using the FLEXible PARTicle~~
422 ~~dispersion model (FLEXPART) in backward mode (Stohl et al., 1998). NOAA Climate Forecast~~
423 ~~System (CFS) short duration ($t < 6$ h) forecasts (Saha et al., 2014) were used as three-dimensional~~
424 ~~forcing datasets. Particle releases from 35-m above sea level (ASL) followed the vessel track using~~
425 ~~vessel position information from the European Common Automatic Weather Station (EUCAWS;~~
426 ~~<http://eumetnet.eu/>; last access Sept. 2021).~~

427 ~~3 Results and Discussion~~

428 ~~3.1 Characteristics of INPs Observed During AQABA~~

429 ~~3.1 Characteristics of INP INP Concentrations s Observed in Aerosol During AQABA~~

430
431 A total of 26 aerosol samples were collected ~~in~~ July – August 2017 during AQABA for offline
432 measurements of INPs. The INP concentrations (n_{INP}) measured in samples collected in the
433 Mediterranean Sea, the Red Sea, the Gulf of Aden, Arabian Sea, Gulf of Oman, and Arabian Gulf
434 spanned up to ~~23~~ orders of magnitude at -15 °C (Fig. 1, Table 1), ~~between 5×10^{-3} and 5×10^{-1} L⁻¹~~
435 ~~¹. This range agrees within an order of magnitude with that of~~ (Prodi et al., (1983) ~~who measured~~

Formatted: Font: Not Italic

Formatted: Font: Not Bold

Formatted: Font: Not Bold

Formatted: Font: Not Bold

Formatted: Font: Not Bold

436 *n*_{INP} in the Mediterranean, Red Sea, Gulf of Aden and Indian Ocean nearly 4 decades prior to the
437 present study (4×10^{-2} to 2 L_μ^{-1} at $-16 \text{ }^\circ\text{C}$). Average ambient dust concentrations during each
438 sampling period ranged from 2-490 $\mu\text{g m}^{-3}$ (PM₁₀ Table 1). There is no agreed-upon standard for
439 definition of extreme dust events in the literature, though the 24-hr average WHO or US EPA
440 health standards for average PM₁₀ are commonly used (Gandham et al., 2020; Khaniabadi et al.,
441 2017). Using the US EPA health standard for PM₁₀ as a threshold for extreme events ($150 \mu\text{g m}^{-3}$), 14 of the 26 samples were collected during dust events. This is conservative given the equivalent
442 WHO guideline for PM₁₀ is $50 \mu\text{g m}^{-3}$ (WHO, 2005), in which case 22 of the 26 sampling periods
443 would be classified as dust events. Prior studies have reported comparable PM₁₀ levels during dust
444 events in the region (Gandham et al., 2020; Krasnov et al., 2016; Shahsavani et al., 2012).
445

Formatted: Superscript

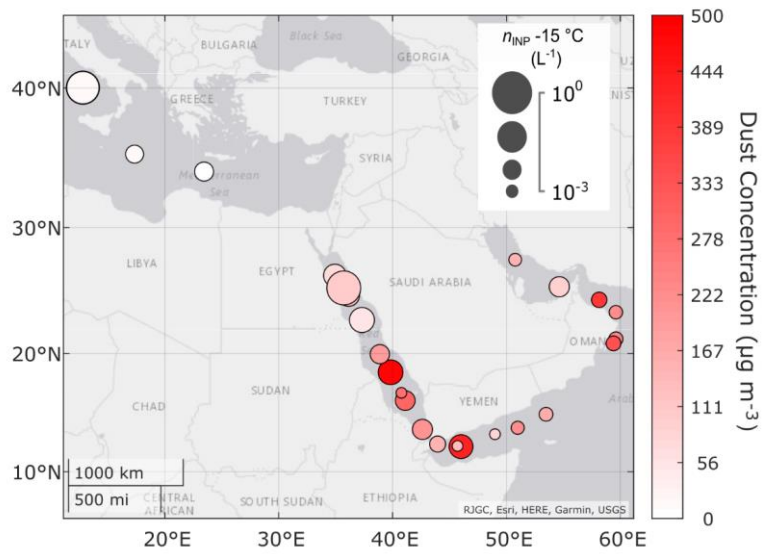
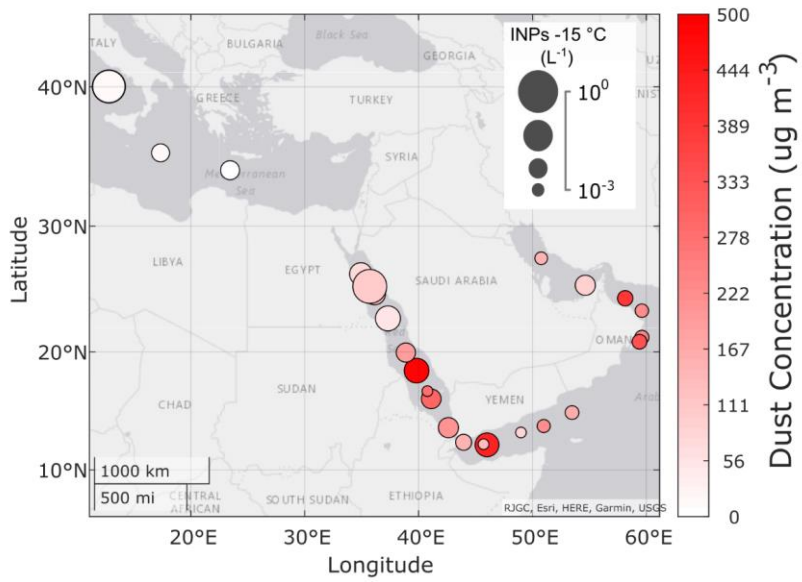
Formatted: Not Superscript/ Subscript

446 Figs. S9-S10 show the extent of k-means clustered FLEXPART back-trajectories below the
447 altitude of 1500 m (see Sect. S5 for details). This threshold was applied to eliminate most of the
448 free tropospheric parts of the back-trajectories and was selected based on the MERRA-2 monthly
449 average planetary boundary layer (PBL) heights during the campaign period, which were 200-700
450 m over the ocean and up to 1700 m over land. FLEXPART ~~72-hour~~ air mass back trajectories
451 show that many ~~of~~ samples collected during extreme dust events (f013, f014, f016, f018, and f020)
452 were influenced by emissions from North Africa and the Arabian Peninsula (Figs S8-S9). Other
453 source regions included the Mediterranean, Nile Delta, Sinai Peninsula (f006-f008, f038),
454 Northeast Egypt (f009-f010), Iran (f023-f024), and Southern and Eastern Europe (f040, f042,
455 f044). The ranges of aerosol surface area concentrations for all sampling periods were $< 320 \mu\text{m}^2$
456 cm^{-3} , with the exception of f024, for which aerosol surface area range was $> 600 \mu\text{m}^2 \text{cm}^{-3}$ (Table
457 1).

Formatted: Font: Not Bold

458

459



462 **Figure 1.** Map of the sample locations for 26 aerosol samples collected on the RV *Kommandor*
 463 *Iona* during Air Quality and climate change in the Arabian Basin (AQABA; [see also Figs. S1-S2](#)
 464 [and S9-S10](#)). Measured n_{INP} concentrations spanned [three](#) orders of magnitude at -15 °C,
 465 from 5×10^{-3} to 5×10^{-1} L⁻¹. Marker sizes indicate abundance of INPs. Marker colors indicate
 466 the average ambient dust mass concentration during the sampling period from hourly MERRA-2
 467 reanalysis data.

468

469 **Table 1.** Summary of aerosol samples collected during AQABA. “—” indicates where data are
 470 missing; “NaN” indicates values below detection limit. Locations are given at the transect
 471 midpoint during each sampling period.

Formatted: Font: 12 pt

Formatted: Justified

Sample ID	Start datetime (UTC)	Stop datetime (UTC)	Latitude (° N)	Longitude (° E)	n_{INP} 15 °C (L ⁻¹)	Sample Volume (L air)	Average Aerosol Surface Area (PM ₁₀ , μm ² cm ⁻³)	Aerosol Surface Area [min, max] (PM ₁₀ , μm ² cm ⁻³)	Average Dust Concentration (PM ₁₀ , μg m ⁻³)	Average Seasalt Concentration (PM ₁₀ , μg m ⁻³)
f006	05-Jul 05:46	05-Jul 11:37	26.224	35.025	0.0146	3370	290	[199, 375]	170	-
f007	05-Jul 16:40	05-Jul 19:51	26.291	34.933	0.0475	2588	260	[222, 289]	70	-
f008	06-Jul 07:09	06-Jul 14:08	25.225	35.775	0.1161	5225	177	[106, 259]	100	-
f009	07-Jul 05:50	07-Jul 15:07	25.011	35.947	0.0838	6940	352	[253,416]	110	-
f010	08-Jul 16:33	09-Jul 05:59	23.623	36.931	0.0592	8073	219	[163, 287]	50	-
f013	14-Jul 12:26	14-Jul 16:13	18.687	39.672	0.0585	2283	264	[176, 352]	490	10
f014	15-Jul 05:10	15-Jul 11:49	16.552	40.834	0.0348	4000	271	[204, 343]	300	5
f016	18-Jul 07:04	18-Jul 14:52	11.939	45.334	0.0534	4690	265	[158, 391]	430	-
f018	22-Jul 10:20	22-Jul 18:44	20.941	59.474	0.0166	5025	212	[171, 238]	340	-
f019	23-Jul 04:48	23-Jul 13:34	21.410	59.691	0.0145	5270	218	[190, 240]	240	-
f020	25-Jul 17:15	26-Jul 04:02	23.976	58.809	0.0184	6511	-	-	390	5
f023	04-Aug 04:05	04-Aug 11:56	28.084	50.284	0.0112	4720	835	[756, 965]	150	4
f024	05-Aug 05:57	05-Aug 13:53	25.432	53.853	0.0371	5221	357	[206, 827]	90	-
f025	07-Aug 09:26	07-Aug 16:46	23.814	59.186	0.0129	4410	55	[46, 72]	220	12
f030	13-Aug 07:08	14-Aug 11:06	15.970	54.705	0.0132	15111	28	[16, 144]	160	-
f031	14-Aug 15:03	15-Aug 09:03	14.003	52.357	0.0121	12972	25	[19, 105]	230	-
f032	15-Aug 09:42	15-Aug 15:07	13.354	49.432	0.0059	3260	96	[82, 147]	80	6
f033	16-Aug 09:30	16-Aug 13:17	12.208	45.706	NaN	2280	73	[51, 135]	130	2

Formatted Table

f034	16-Aug 13:27	17-Aug 07:04	12.177	45.429	0.0206	8464	168	[51, 372]	150	1
f035	17-Aug 07:30	17-Aug 14:55	13.308	42.974	0.0365	4460	340	[244, 409]	210	2
f036	18-Aug 06:36	18-Aug 15:03	16.290	41.038	0.0057	6634	208	[160, 428]	280	2
f037	19-Aug 07:05	20-Aug 07:04	18.699	39.609	0.0326	18806	240	[175, 331]	190	7
f038	21-Aug 07:22	21-Aug 16:01	24.112	36.554	0.0422	6700	256	[202, 295]	150	-
f040	26-Aug 16:02	27-Aug 07:04	33.803	24.814	0.0314	9030	90	[58, 142]	< 10	3
f042	28-Aug 07:51	28-Aug 16:02	35.310	17.965	0.0279	6396	163	[131, 222]	< 10	2
f044	31-Aug 08:30	31-Aug 20:16	39.569	13.380	0.4572	11296	211	[148, 255]	< 10	-

Sample ID	Start_datetime (UTC)	Stop_datetime (UTC)	Latitude	Longitude	Sample Volume (L-air)	Aerosol Surface Area ($\mu\text{m}^2 \text{cm}^{-3}$)	Average Dust Concentration ($\mu\text{g m}^{-3}$)	Average Seasalt Concentration ($\mu\text{g m}^{-3}$)	
				0.0146				Formatted: Font: (Default) Times New Roman, 8 pt	
f006unt	05-Jul-05:46	05-Jul-11:37	26.224	35.025	0.0475	3370	290	170	Formatted: Font: (Default) Times New Roman, 8 pt
f007unt	05-Jul-16:40	05-Jul-19:51	26.291	34.933	0.1161	2588	260	70	Formatted: Font: (Default) Times New Roman, 8 pt
f008unt	06-Jul-07:09	06-Jul-14:08	25.225	35.775	0.0838	5225	180	100	Formatted: Font: (Default) Times New Roman, 8 pt
f009unt	07-Jul-05:50	07-Jul-15:07	25.011	35.947	0.0592	6940	350	110	Formatted: Font: (Default) Times New Roman, 8 pt
f010unt	08-Jul-16:33	09-Jul-05:59	23.623	36.931	0.0585	8073	220	50	Formatted: Font: (Default) Times New Roman, 8 pt
f013unt	14-Jul-12:26	14-Jul-16:13	18.687	39.672	0.0348	2283	260	490	Formatted: Font: (Default) Times New Roman, 8 pt
f014unt	15-Jul-05:10	15-Jul-11:49	16.552	40.834	0.0534	4000	270	300	Formatted: Font: (Default) Times New Roman, 8 pt
f016unt	18-Jul-07:04	18-Jul-14:52	11.939	45.334	0.0166	4690	260	430	Formatted: Font: (Default) Times New Roman, 8 pt
f018unt	22-Jul-10:20	22-Jul-18:44	20.941	59.474	0.0145	5025	210	340	Formatted: Font: (Default) Times New Roman, 8 pt
f019unt	23-Jul-04:48	23-Jul-13:34	21.410	59.691	0.0184	5270	220	230	Formatted: Font: (Default) Times New Roman, 8 pt
f020unt	25-Jul-17:15	26-Jul-04:02	23.976	58.809	0.0112	6511	-	390	Formatted: Font: (Default) Times New Roman, 8 pt
	04-Aug	04-Aug							
f022unt	04:05	11:56	28.084	50.284	0.0371	4720	830	150	Formatted: Font: (Default) Times New Roman, 8 pt
	05-Aug	05-Aug							
f024unt	05:57	13:53	25.432	53.853	0.0129	5221	360	90	Formatted: Font: (Default) Times New Roman, 8 pt
	07-Aug	07-Aug							
f025unt	09:26	16:46	23.814	59.186	0.0132	4410	50	220	Formatted: Font: (Default) Times New Roman, 8 pt
	13-Aug	14-Aug							
f030unt	07:08	11:06	15.970	54.705	0.0121	15111	30	160	Formatted: Font: (Default) Times New Roman, 8 pt
	14-Aug	15-Aug							
f031unt	15:03	09:03	14.003	52.357	0.0059	12972	30	220	Formatted: Font: (Default) Times New Roman, 8 pt

f032unt	15-Aug 09:42	15-Aug 15:07	13.354	49.432	NaN	3260	100	80	Formatted: Font: (Default) Times New Roman, 8 pt
f033unt	16-Aug 09:30	16-Aug 13:17	12.208	45.706	0.0206	2280	90	130	Formatted: Font: (Default) Times New Roman, 8 pt
f034unt	16-Aug 13:27	17-Aug 07:04	12.177	45.429	0.0365	8464	170	150	Formatted: Font: (Default) Times New Roman, 8 pt
f035unt	17-Aug 07:30	17-Aug 14:55	13.308	42.974	0.0057	4460	340	210	Formatted: Font: (Default) Times New Roman, 8 pt
f036unt	18-Aug 06:36	18-Aug 15:03	16.290	41.038	0.0326	6634	210	280	Formatted: Font: (Default) Times New Roman, 8 pt
f037unt	19-Aug 07:05	20-Aug 07:04	18.699	39.609	0.0422	18806	240	190	Formatted: Font: (Default) Times New Roman, 8 pt
f038unt	21-Aug 07:22	21-Aug 16:01	24.112	36.554	0.0314	6700	260	140	Formatted: Font: (Default) Times New Roman, 8 pt
f040unt	26-Aug 16:02	27-Aug 07:04	33.803	24.814	0.0279	9030	90	<10	Formatted: Font: (Default) Times New Roman, 8 pt
f042unt	28-Aug 07:51	28-Aug 16:02	35.310	17.965	0.4572	6396	160	10	Formatted: Font: (Default) Times New Roman, 8 pt
f044unt	31-Aug 08:30	31-Aug 20:16	39.569	13.380	$n_{\text{INP}}^{-15^\circ\text{C}}$ (L ⁻¹)	11296	210	10	Formatted: Font: (Default) Times New Roman, 8 pt

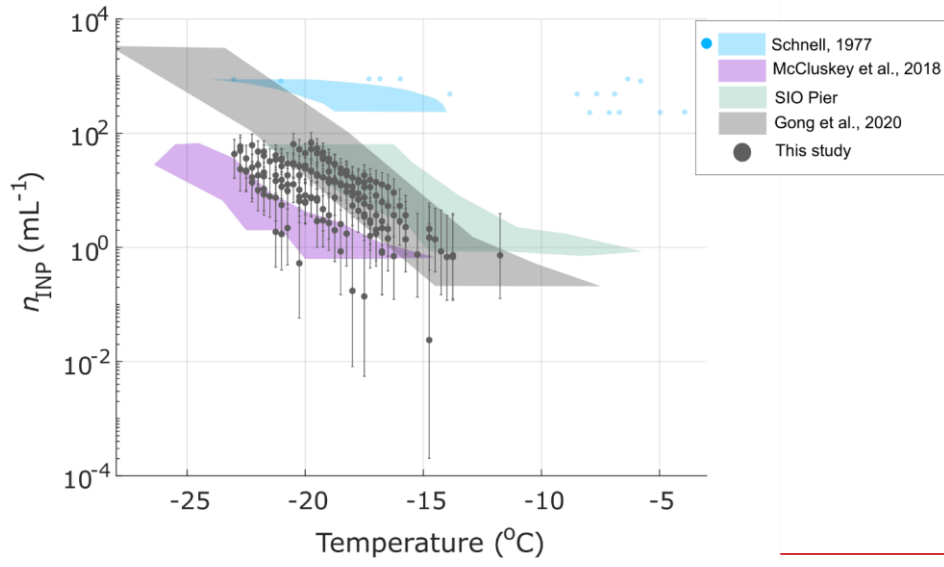
472 3.2 Seawater Source Potential

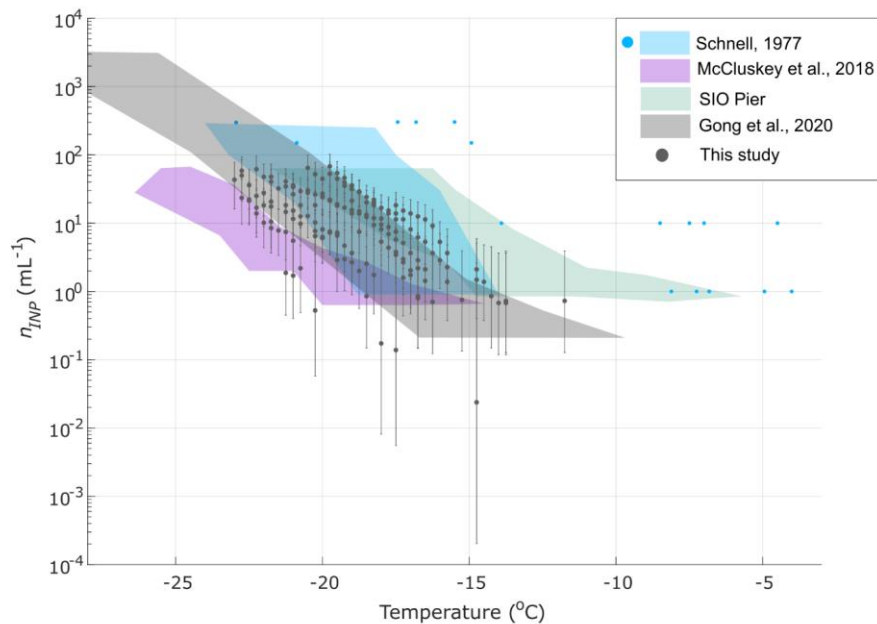
473 The n_{INP} values in 10 SSW samples collected during AQABA were used to characterize the INP
474 source potential of SSA generated by bubble bursting (Wang et al., 2017). Results from prior
475 studies have demonstrated that jet droplets are a more efficient transfer vehicle than film drops of
476 INPs into SSA particles (Mitts et al., 2021; Wang et al., 2017). We measured the n_{INP} in SSW to
477 test whether the seawater source strength was comparable to that of prior studies, or whether the
478 SSW was possibly enriched with INPs due to biological activity or even dust deposition (Cornwell
479 et al., 2020).

480 Figure S11 shows how the n_{INP} measured at -19 °C in 10 seawater samples varied by the sample
481 collection location. Concentrations ranged between 1 and 50 n_{INP} mL⁻¹ and were highest between
482 the Gulf of Oman and the Gulf of Aden. This region exhibited relatively high chlorophyll *a* during
483 the cruise, with levels between 1 and 30 mg m⁻³ (Fig. S12). In Fig. 2, n_{INP} were compared with
484 SSW from the Ellen Browning Scripps Memorial Pier in coastal Southern California (SIO Pier).

485 Cabo Verde in the Northeast Atlantic, the Southern Ocean (McCluskey et al., 2017), and the
486 Northwest Atlantic (Schnell, 1977). AQABA n_{INP} were most comparable with Gong et al.'s
487 (2020) observations in Cabo Verde. The lack of any unusually high INP spectra suggests that INP
488 enrichment due to dust deposition (Cornwell et al. 2020) was absent or infrequent. It is possible
489 that storage of SSW samples (Sect. 2.5) could have decreased measured n_{INP} , though we expect

490 that n_{INP} would be decreased by no more than 10× in untreated samples stored frozen (see
491 [discussion below](#)).





493
 494 **Figure 2.** Measured n_{INP} in 10 SSW samples collected during AQABA. Also shown are the
 495 composite INP spectrum of 14 coastal SSW samples collected on São Vicente Island, Cabo Verde
 496 (Gong et al., 2020), 17 coastal SSW samples collected at the Ellen Browning Scripps Pier (green
 497 shading), and 12 SSW samples collected in the Southern Ocean (McCluskey et al., 2018d).
 498 Schnell's (1977) SSW measurements are represented as a composite spectrum of 24 samples (blue
 499 shaded region) and 5 additional spectra (blue markers) from samples that exhibited higher freezing
 500 temperatures. All spectra presented are uncorrected for freezing point depression.

501 Offline treatments for testing heat lability, organic composition, and size were applied to 5 of the
 502 10 seawater samples (Methods Sec. 2.5). Heat and 0.2 μm filtering treatments suggest that a large
 503 fraction of the seawater INPs were heat sensitive and larger than 0.2 μm (Fig. S13). These results
 504 are indicative of the POC type of marine INP defined in McCluskey et al. (2018a), though this
 505 result should be interpreted with caution as storage could potentially have increased sensitivity to
 506 filtering treatments.

- Formatted: Font: (Default) Times New Roman, 12 pt
- Formatted: Normal
- Formatted: Font: (Default) Times New Roman, 12 pt, Bold
- Formatted: Font: (Default) Times New Roman, 12 pt
- Formatted: Font: (Default) Times New Roman, 12 pt
- Formatted: Font: Bold

507 Understanding of storage impacts on INPs measured in SSW is lacking. However, Beall et al.,
508 (2020) showed that average INP concentration changes for untreated coastal precipitation samples
509 due to frozen storage were within 2× of n_{INP} measured in fresh samples, with changes at the upper
510 or lower end of the 95% CI exceeding 10× for some freezing temperatures. If SSW samples are
511 similarly sensitive to storage, we would expect INP concentration changes to be within 2× on
512 average, but up to > 10× for any particular untreated sample. Beall et al. (2020) also reported
513 similar changes INPs < 0.45 μm with a greater tendency toward losses, which indicates that storage
514 may have caused increased sensitivity to the filter treatments applied to stored samples.

Formatted: Justified

515 **3.3 Ice-active Surface Site Densities in Aerosol**

516 In Figure 32, approximated ice ~~nucleation~~-active surface site densities (n_s) in aerosol samples are
517 compared with multiple population-specific observations and parameterizations for dust and
518 marine INPs. The AQABA measurements are also compared with observations from dust-laden
519 air over the Tropical Atlantic (Price et al., 2018). Overall, observations nearly bridge the full
520 regime between the M18 parameterization for marine INPs (~~hereafter "M18"~~; McCluskey et al.,
521 2018c), and multiple dust INP parameterizations based on laboratory studies of surface dust. At
522 higher temperatures, between -5 and -12 °C, most observations show agreement with the
523 composite spectrum of n_s observed in a range of marine and coastal environments from DeMott et
524 al. (2016) and ~~(Yang et al., (2020) Yang et al. (2019)~~, and/or the ~~Atkinson et al. (2013)~~ A13 K-
525 feldspar parameterization. Between -10 and -20 °C, several samples agree with the M18 marine
526 INP parameterization within an order of magnitude, whereas two to three n_s spectra approach the
527 U17 and N12 laboratory-derived dust INP parameterizations within an order of magnitude
528 (Niemand et al., 2012; Ullrich et al., 2017), depending on temperature. Multiple samples (~8)
529 additionally agreed with Price et al.'s (2018) observations of INPs between 30-3500 m above the
530 ~~dust-laden~~ Tropical Atlantic, and most agree with the Gong et al. (2020) surface-level
531 observations, measured at Cabo Verde in the same region ~~as Price et al. (2018) (Cabo Verde)~~.

Formatted: Font: Bold

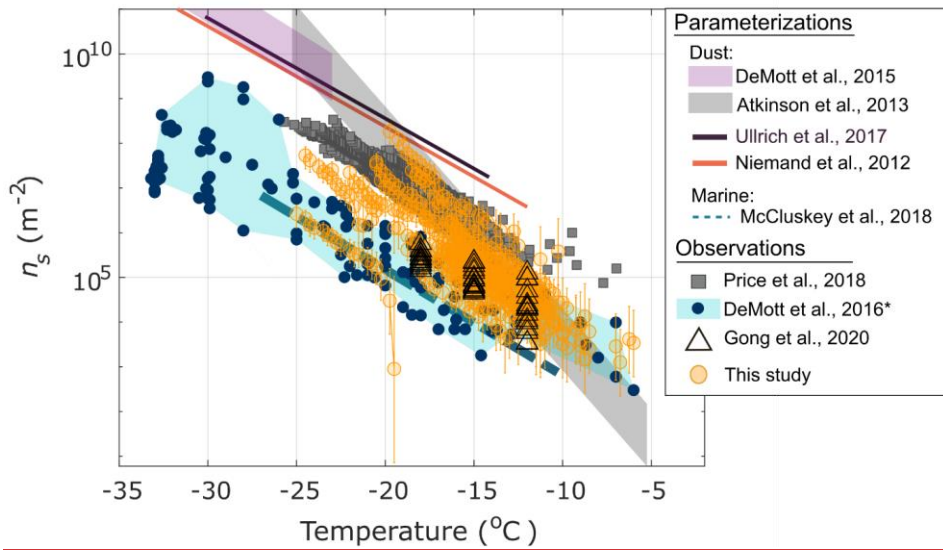
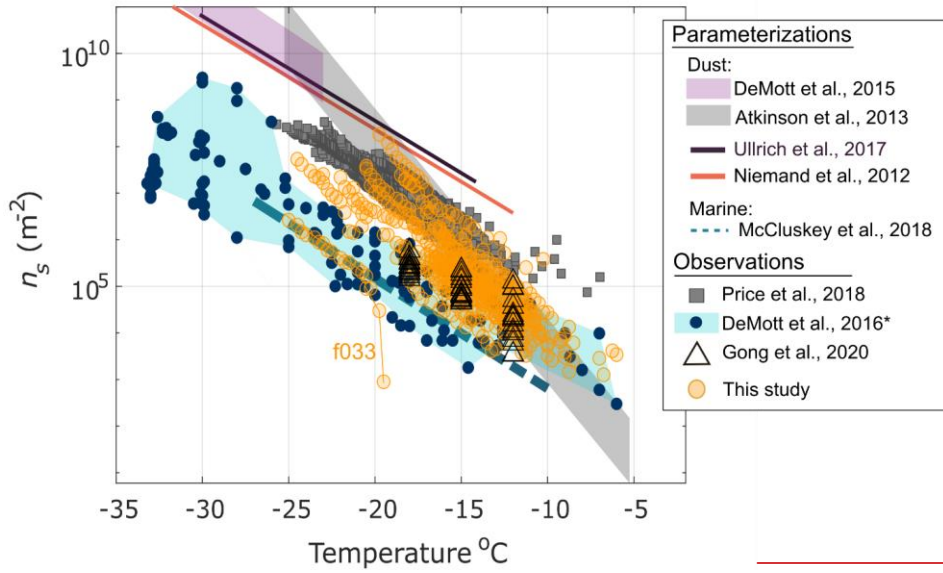
Formatted: Font: Bold

Formatted: Font: Bold

Formatted: Font: Bold

Formatted: Font: Bold

Formatted: Font: Bold



534 **Figure 32.** Ice-active surface nucleation-site densities (n_s) as a function of temperature for 25 of
535 26 aerosol samples collected during AQABA. Gong et al. (2020) and Price et al. (2018) measured
536 INPs in dust-dominant air masses in the tropical east Atlantic, with minor contributions from SSA,
537 while the DeMott et al. (2016) measurements were collected across a range of locations and
538 conditions within the marine boundary layer comprising air masses mostly dominated by relatively
539 pristine marine SSA. INP concentrations measured in sample f033 were below the detection limits
540 imposed by field blanks (see Sect. 2.4, Fig. S76). Error bars represent 95% binomial sampling
541 confidence intervals (Agresti and Coull, 1998). Sample f020 is not shown due to missing aerosol
542 surface area data during the sampling period. For the 8 samples on which a dilution was performed
543 (Fig. S8), n_s for both the raw undiluted and diluted sample are shown. *DeMott et al. (2016) data
544 shown have been updated with additional data from Yang et al. (2020).

Formatted: Justified

546 Considering the frequency of dust events encountered (dust concentration > 150 $\mu\text{g m}^{-3}$, see Table
547 1), and the high probability that dust was the dominant aerosol source during most sampling
548 periods, it is striking that most n_s spectra observed are 1-3 orders of magnitude lower than the
549 values predicted by dust parameterizations. As noted in Gong et al. (2020), some deviations could
550 be expected due to the difference between approximated n_s based on total particle surface area in
551 ambient measurements and true n_s based on surface area of a homogeneous aerosol population (see
552 Methods Sect. 2.4). The FLEXPART back trajectories show that air masses for multiple samples
553 originated from densely populated regions such as Southern and Eastern Europe (f040, f042, f044,
554 Fig S9). The back trajectories also show that for samples f006 f008, f010, and f038, air masses
555 were influenced by the populous region around the Nile River Delta. Agricultural soil dusts
556 represent a potential constituent of the INPs observed from these regions. A range of n_s has been
557 reported in studies of agricultural soil dusts, the lower end of which agrees with the n_s observed in
558 the present study between 8 and 25 °C (Steinke et al., 2016; Tobo et al., 2014; O'Sullivan et al.,
559 2014).

Formatted: Superscript

560 Given the marine environment in which sampling occurred took place, a significant amount of sea
561 spray aerosol (SSA) was also detected in many of the sampled airmasses, using sea salt as a proxy
562 (Table 1), and likely present in others for which no composition data were available. Edtbauer et
563 al. (2020) reported the detection of high levels of dimethyl sulfide (DMS, up to 800 ppt) in the

Formatted: Justified

564 Gulf of Aden associated with a local phytoplankton bloom during AQABA (as evidenced by
565 visible bioluminescence around the ship at night) as well as high levels of dimethyl sulfone
566 (DMSO₂) and other marine biogenic volatile organic carbons (VOCs) from the Somalian
567 upwelling region. As mentioned above, the n_s for most samples between -6 and -18 °C agree with
568 n_s derived from observations across various locations within the marine boundary layer (Fig. 3.2).
569 However, considering that SSA is associated with 1000 times fewer IN sites per unit surface area
570 than dust (i.e. 1000× lower n_s) (McCluskey et al., 2018c), the characteristically low IN activity of
571 untreated SSW (even in light of the modest changes expected from storage, Sect. 3.2), and the
572 frequency of dust events during AQABA, our findings suggest it is unlikely that the observed INPs
573 originated from SSA, and the high relative abundance of dust compared to sea salt concentrations
574 (Table 1), it is unlikely that the observed INPs originated from SSA. In general, detection of marine
575 INPs in ambient aerosol is challenging due to their low relative abundance and decreased
576 efficiency compared to dust (DeMott et al., 2016; McCluskey et al., 2018c). Thus, while SSA
577 contributed to the measured aerosol surface area (Table 1), it is unlikely that the INPs observed in
578 this study were marine in origin, or at least that this is indiscernible in the present study or based
579 on present parameterizations of these populations.

Formatted: Not Superscript/ Subscript

580 Heterogeneous aerosol composition in the sampled air masses likely contributed to some of the
581 low n_s spectra observed due to the contribution of non-INPs to the measured aerosol surface area
582 (see description of n_s approximation in Sect. 2.4). However, the difference between n_s observed
583 during the most extreme dust events, i.e., when the aerosol population was likely approaching
584 homogeneity in composition, and the n_s predicted from N12 and U17 was still greater than 2 orders
585 of magnitude. Figures 4.3(a) and (b) show overlap in n_{INP} and n_s observed in samples collected in
586 low dust and high dust conditions, indicating that the INP populations observed during AQABA
587 exhibited similar efficiencies-IN activity despite variation in total aerosol composition and dust
588 loading. No correlation was found between n_{INP} and aerosol surface area (Fig. S147), PM₁₀ or dust
589 concentration. This result is in contrast to Price et al. (2018) who found the variability in n_{INP} to
590 be largely determined by variability in dust loading or aerosol surface area. (Price et al., (2018)
591 reported higher maximum aerosol surface area concentrations of ~1500 $\mu\text{m cm}^{-3}$ from three
592 samples collected in an exceptionally optically thick layer, compared to the maximum of 965 μm
593 cm^{-3} in the present study (Table 1). Yet overall, the aerosol surface area concentrations compare
594 very well with those observed by (Price et al., 2018), indicative of comparable dustiness in the two

Formatted: Font: Not Italic

Formatted: Font: Not Italic

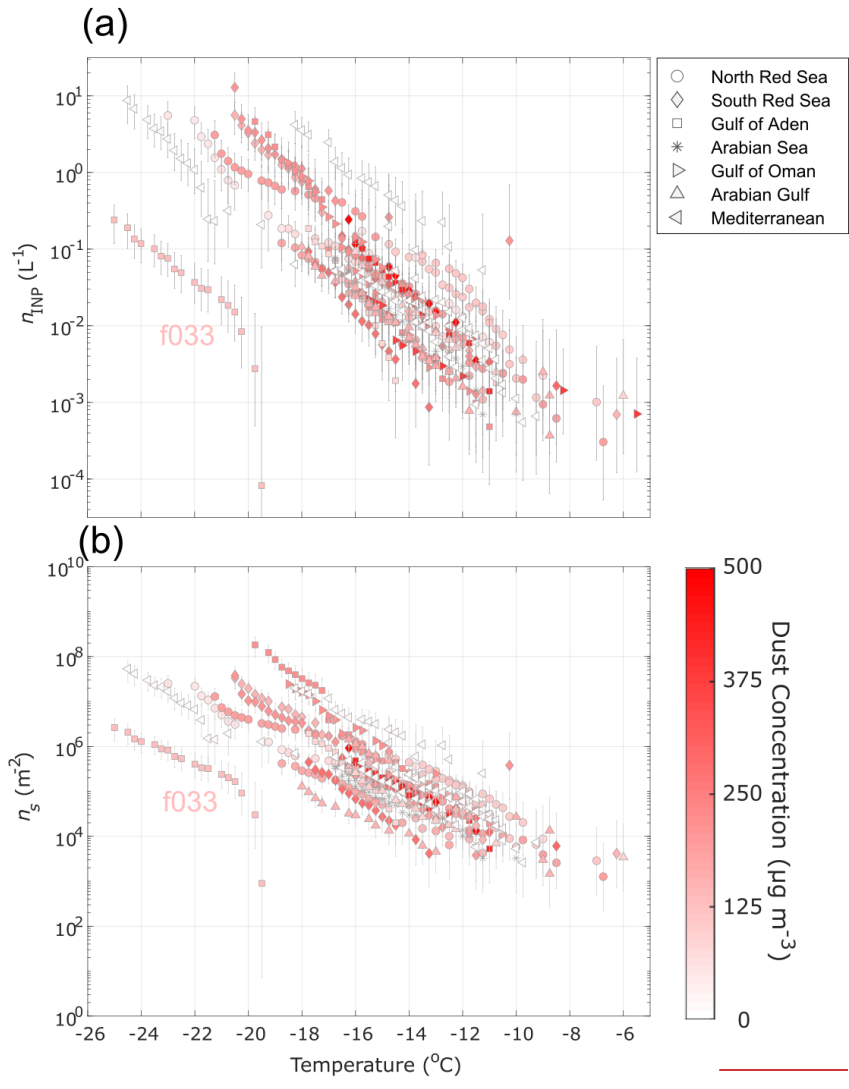
Formatted: Subscript

Formatted: Font: Not Italic

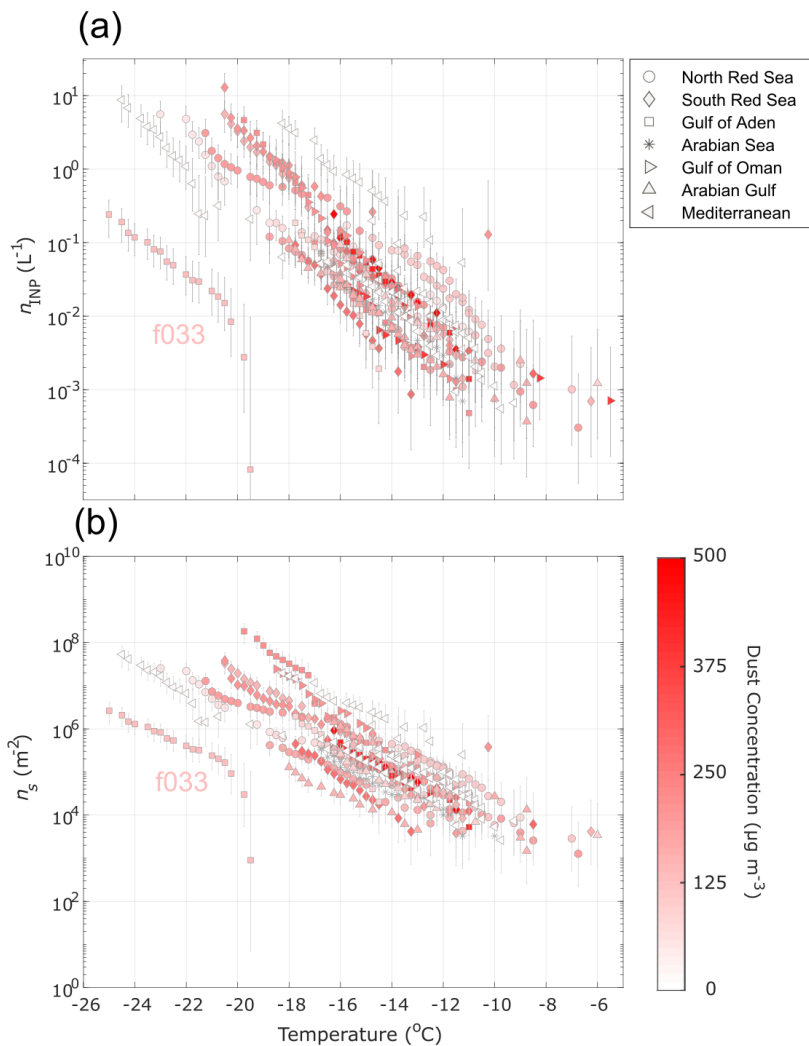
Formatted: Superscript

595 studies. Excluding ~~the three case mentioned above samples, Price et al. (2018) collected in an~~
596 ~~exceptionally optically thick dust layer~~, the average aerosol surface area was $227 \pm 68 \mu\text{m}^2 \text{cm}^{-3}$
597 vs. $226 \pm 26 \mu\text{m}^2 \text{cm}^{-3}$ for the present study. Furthermore, the sample with the highest n_s at $-15 \text{ }^\circ\text{C}$
598 (f0440) was collected when dust concentrations were lowest ($< 10 \mu\text{g m}^{-3}$) (Fig. 43, Table 1).
599 This is also in direct contrast to Price et al. (2018), who found that the highest n_s observed
600 corresponded to the highest dust loading.

601 ~~Gong et al. (2020) also observed n_s lower by more than 2 orders of magnitude compared to N12~~
602 ~~and U17 despite the large fraction of supermicron INPs (77–83% depending on temperature), and~~
603 ~~that the supermicron particles were mainly mineral dust. The large differences between~~
604 ~~parameterized n_s for dust, and n_s observed in both Gong et al. (2020) and the present study between~~
605 ~~-12 and $-25 \text{ }^\circ\text{C}$ demonstrate that existing n_s -based parameterizations may not faithfully represent~~
606 ~~n_s at moderate freezing temperatures, despite proximity to major source regions. Whereas DeMott~~
607 ~~et al. (2015a) found that for temperatures $< 20 \text{ }^\circ\text{C}$, mineral dust particles from Saharan and Asian~~
608 ~~deserts may be parameterized as a common particle type, our findings suggest that characteristic~~
609 ~~n_s parameterizations for dust from different source regions may be needed $> 20 \text{ }^\circ\text{C}$, or,~~
610 ~~alternatively, that this temperature regime requires an alternative to an n_s -based parameterizations.~~
611 ~~Gong et al. (2019a) demonstrated that predicting n_{INP} from surface area size distributions alone~~
612 ~~may not be feasible in environments where the aerosol and/or INP composition are unknown and~~
613 ~~proposed a probability density function PDF-based approach to predicting INPs at a given freezing~~
614 ~~temperature.~~



615 -



616
 617 **Figure 43.** INP concentrations (n_{INP}) (a) and ice-nucleation-active surface site densities (n_s) (b)
 618 as a function of temperature for 26 aerosol samples collected during AQABA. Markers are colored
 619 by the average ambient dust concentration for the respective sampling period. Error bars represent
 620 95% binomial sampling confidence intervals (Agresti and Coull, 1998). The n_s measured in
 621 samples collected during low dust conditions are equal to or greater than (up to 100×) the n_s

Formatted: Font: Not Italic

Formatted: Font: Not Bold

Formatted: Font: Not Bold

Formatted: Font: Not Bold

Field Code Changed

622 measured during dust events between -9 and -18 °C. INP concentrations measured in sample f033
623 were below the detection limits imposed by field blanks (see Sect. 2.4, Fig. S76). Sample f020 is
624 not shown in (b) due to missing aerosol surface area data during the sampling period. For the 8
625 samples on which a dilution was performed (Fig. S8), n , for both the raw undiluted and diluted
626 sample are shown.

Formatted: Font: Not Bold

Formatted: Font: Not Bold

627 3.4 Characterization of INPs in Aerosol

Formatted: Font: Bold

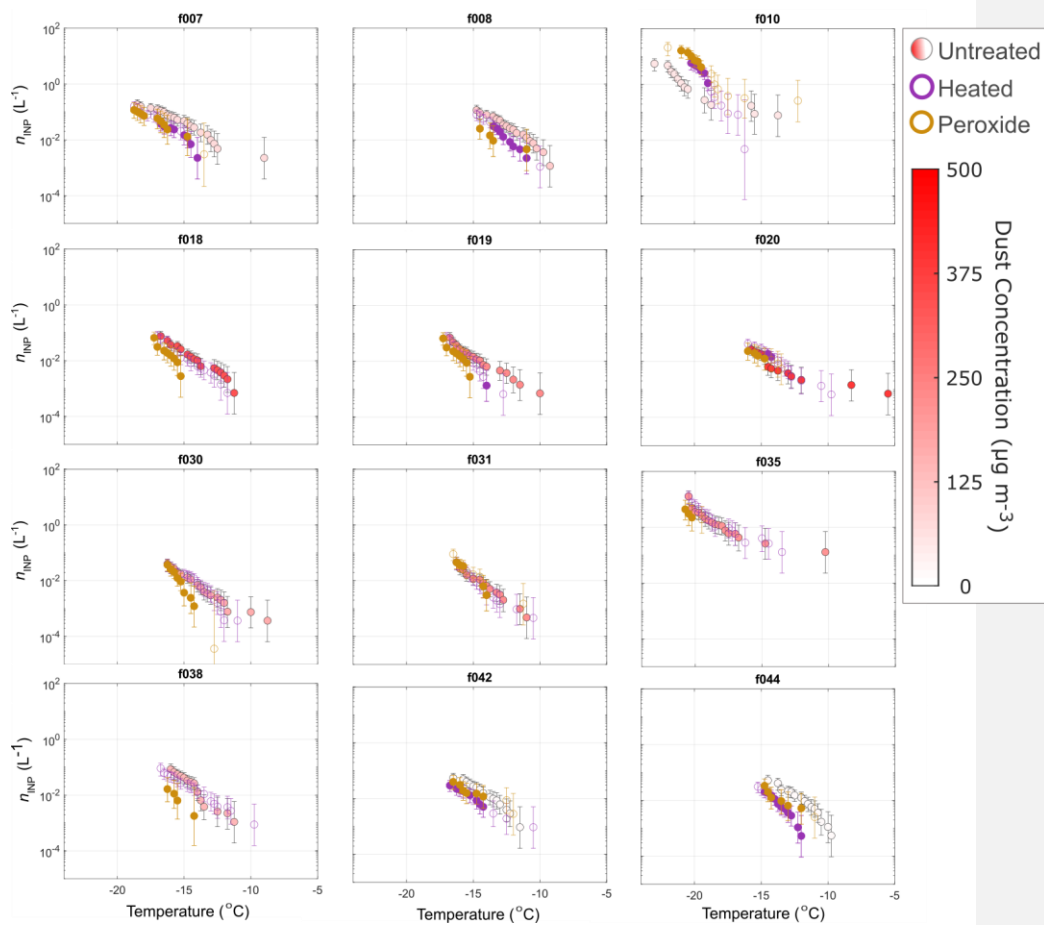
628 Offline treatments for testing heat lability and organic composition of INPs were performed on 12
629 samples via heat and H₂O₂-peroxide treatments, respectively (Fig. 54). Prior studies have shown
630 that the IN-active component of various types of mineral dusts are insensitive to heat treatments
631 (Conen et al., 2011; Hara et al., 2016; Hill et al., 2016; O'Sullivan et al., 2014). The IN activity of
632 K-feldspar, the dominant ice-nucleating component of mineral dust, was additionally found to
633 be insensitive to digestion with peroxide (O'Sullivan et al., 2014). A small number of studies
634 reported degradation of IN activity with peroxide treatment and/or heat treatment in Arizona Test
635 Dust (ATD), that they attributed to organic material (Perkins et al., 2020; Yadav et al., 2019).
636 Thus, we assume here that any degradation of IN activity due to heat and peroxide treatment ~~are~~
637 do correspond to loss of heat-labile (e.g. proteinaceous) and heat-stable organic INPs,
638 respectively.

639 Fisher's Exact Test was applied to frozen and unfrozen well fractions for each untreated sample
640 and its corresponding treated sample to test for significant differences ($p < 0.05$). Sensitivity to
641 peroxide in most samples (i.e., INP degradation) demonstrate the consistent presence of stable
642 organic INPs at temperatures ≥ -15 °C. The lack of peroxide sensitivity at temperatures <below -
643 15 °C indicates dominance by mineral dust INPs at lower temperatures. Heat sensitivity in five
644 samples suggests that biological INPs contributed to their warmest freezing INPs. Gong et al.
645 (2020) similarly found heat-sensitivity in INPs at temperatures > -10 °C. Four of the 12 samples
646 exhibited heat sensitivity at relatively moderate temperatures -11 to -18 °C, including the two
647 samples collected in the Mediterranean Sea. One sample (f010) exhibited increased $n_{\text{INP_INP}}$
648 concentrations in freezing temperatures <below -18 °C after heat and peroxide treatments. That
649 the response to both heat and peroxide were nearly identical (Fig. 54) suggests that compounds
650 may have been released from the surface during heating, uncovering a more IN active surface

651 underneath (heating was common to both procedures). The increased η_{NP} post heat and peroxide
652 treatment is an unexpected result given previous studies on treated soil dust measurements (Conen
653 et al., 2011; Hill et al., 2016; O’Sullivan et al., 2014; Tobo et al., 2014). However, increases in IN
654 activity after heat treatment have been reported previously for airborne Saharan desert dust and
655 aerosol collected during Saharan dust intrusions (Boose et al., 2019; Conen et al., 2022) as well as
656 SSA and precipitation (Martin et al., 2019; McCluskey et al., 2018a) and should be further
657 investigated in future studies. ~~though an~~ An increase in IN activity after peroxide treatment has

Formatted: Font: Not Italic

658 also been reported in a Himalayan dust sample (Paramonov et al., 2018). -peroxide treatment has
659 also been reported in a Himalayan dust sample (Paramonov et al., 2018).



660
661 **Figure 54.** INPs in aerosol samples treated with heat and H₂O₂-peroxide (Methods Sec. 2.4) to test
662 for INP heat-lability and organic composition. Markers of untreated spectra are colored by the
663 average dust concentration during the sampling period. Markers of heat-treated and H₂O₂-peroxide-
664 treated samples are filled to indicate significant INP concentration difference from untreated
665 samples according to Fisher's Exact Test ($p < 0.05$). Sensitivity to H₂O₂-peroxide is evident for all
666 samples ≥ -15 °C, indicative of stable organic INPs. Heat-lability is also evident at high to

667 moderate temperatures in multiple samples, demonstrating that biological (e.g., proteinaceous)
668 INPs also contributed to INPs observed during AQABA.

669 Given the frequency of dust ~~storms events~~ and generally high concentrations of dust during most
670 sampling periods, it is surprising that most samples exhibit peroxide sensitivity. Aridisols and
671 entisols are the dominant soil types in North Africa and the Arabian Peninsula (Nortcliff, 2012).
672 Both types are associated with the lowest levels of organic carbon, commonly used as a proxy for
673 total soil organic matter, compared to other soil types (3 and 9 g kg⁻¹, respectively) (Yost and
674 Hartemink, 2019).

675 **3.5 Characterization of INPs in a Soil Dust Sample**

676 INP measurements of soil dusts in this region are scarce and have only been reported for a single
677 surface dust soil sample, sample “SD”, collected 50 km north of Cairo (Niemand et al., 2012).
678 ~~FLEXPART back-trajectories indicate this source region for several samples (f006-10, f038),~~
679 ~~though it should be noted that dust sources cannot be confirmed in this study lacking aerosol and~~
680 ~~soil dust minerology.~~ For comparison with this study, we measured INPs in untreated, heat-treated,
681 and peroxide-treated subsamples of an archived ~~aliquot suspension~~ of the ~~N12--SD~~ sample
682 ~~(Methods Sect. 2.4; DeMott et al., 2018) described in Niemand et al. (2012),~~ Sample ~~N12-SD~~
683 exhibits sensitivity to both heat and peroxide at temperatures > -16 °C, indicating biological
684 composition of INPs at high freezing temperatures. Multiple AQABA samples influenced by
685 desert air mass sources show similar sensitivities at higher temperatures: f006, f007, f019, and
686 f020. Several others exhibit only peroxide-sensitivity in this temperature range. Overall, the heat
687 and peroxide sensitivities in the ~~N12-SD~~ sample indicate that desert dusts may contribute
688 biological and/or organic INPs at moderate to high-freezing temperatures, such as those observed
689 in AQABA samples. Gong et al.'s (2020) results showing heat-sensitivity in INPs at temperatures
690 > -10 °C further demonstrate the contribution of biological INPs at high temperatures in dust-
691 ~~laden~~ air masses near ~~North-~~ Africa.

Formatted: Font: Bold

Formatted: Font: Bold

Formatted: Font: Bold

Formatted: Font: (Default) Times New Roman, 12 pt

Formatted: Normal

Formatted: Font: (Default) Times New Roman, 12 pt, Bold

Formatted: Font: (Default) Times New Roman, 12 pt

Formatted: Font: (Default) Times New Roman, 12 pt

Formatted: Font: (Default) Times New Roman, 12 pt

Formatted: Font: (Default) Times New Roman, 12 pt

Formatted: Font: (Default) Times New Roman, 12 pt

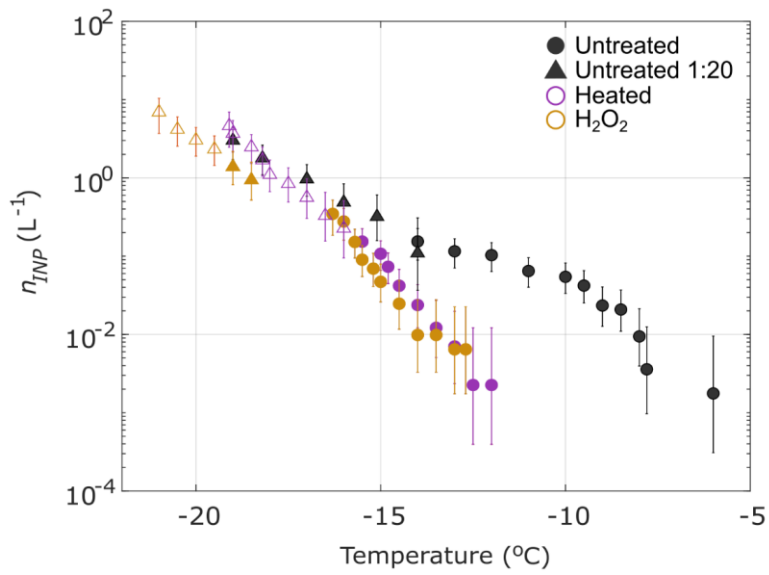
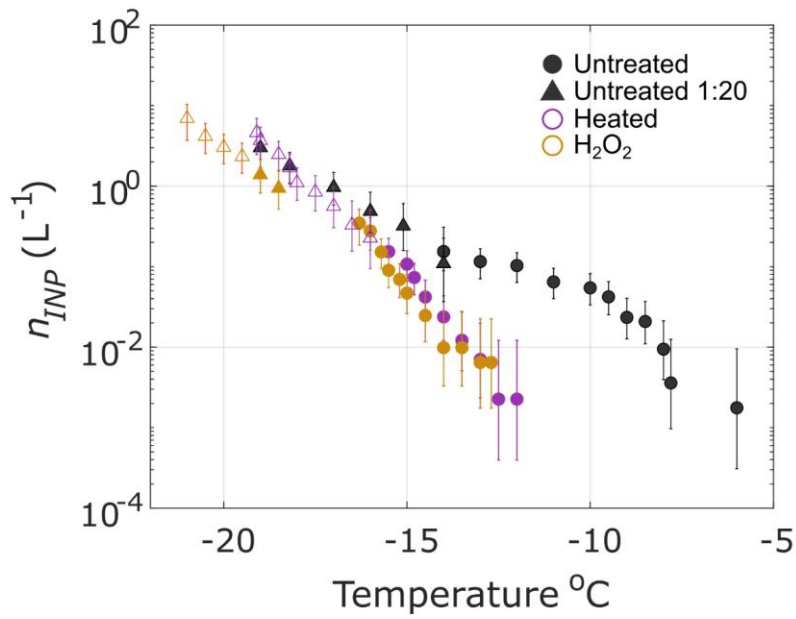
Field Code Changed

Formatted: Font: (Default) Times New Roman, 12 pt

Formatted: Font: (Default) Times New Roman, 12 pt, Bold

Formatted: Font: (Default) Times New Roman, 12 pt

Formatted: Font: 14 pt, Bold



694 **Figure 65.** Measured concentrations of INPs in an aerosolized soil dust sample “N12-SD”
695 collected 50 km north of Cairo, Egypt (Niemand et al., 2012), that was treated with heat and
696 peroxide to test for INP heat-lability and organic composition, same as in Fig. 54 above (Methods
697 Sec. 2.4). A 1:20 dilution of the sample is shown (triangles) and markers of heat-treated and
698 H_2O_2 peroxide-treated samples are filled to indicate significant INP concentration differences from
699 untreated samples according to Fisher’s Exact Test ($p < 0.05$). Sensitivity to peroxide and heat
700 treatments indicates biological INPs between -6 and -16 °C.

701 **4 Discussion**

702 Considering the high freezing temperatures observed, evidence of organic composition, and
703 FLEXPART back trajectories showing that aerosol sources included populous regions and at least
704 one agriculturally active region (the Nile River Delta; Figs. S9-S10), it is possible that agricultural
705 soil dusts contributed to some of the relatively higher n_s , n_{INP} , and heat and peroxide sensitivity
706 observed during AQABA. A range of n_s has been reported in studies of agricultural soil dusts, the
707 lower end of which agrees with the n_s observed in the present study between -8 and -25 °C (Fig.
708 3; Steinke et al., 2016; Tobo et al., 2014; O’Sullivan et al., 2014). Samples from air masses
709 influenced by the Nile River Delta or Southern Europe (f007-8, f010, f038, f042, f044) show a
710 higher fraction of heat-sensitive INPs (Fig. 54). Heat-sensitivity is indicative of biological INPs,
711 which have been associated with agricultural soil dusts in prior studies (Hill et al., 2016;
712 O’Sullivan et al., 2014). Hill et al. (2016) and O’Sullivan et al. (2014) showed peroxide sensitivity
713 in agricultural soil dusts at temperatures > -18 to -15 °C, respectively, a range which aligns with
714 the peroxide sensitivity exhibited in the present study. A range of n_s has been reported in studies
715 of agricultural soil dusts, the lower end of which agrees with the n_s observed in the present study
716 between -8 and -25 °C (Steinke et al., 2016; Tobo et al., 2014; O’Sullivan et al., 2014). Agricultural
717 soil dusts are relatively rich in organic and biological material (Conen et al., 2011, 2016; Ellerbrock
718 et al., 2005; Kögel Knabner et al., 2008; O’Sullivan et al., 2014) and contribute up to 20-25% of
719 the global dust load (Ginoux et al., 2012). Furthermore, they are associated with IN activities
720 higher than that of mineral dust (Conen et al., 2011; Fornea et al., 2009; Isono and Ikebe, 1960;
721 O’Sullivan et al., 2014; Steinke et al., 2016; Tobo et al., 2014). High onset temperatures, up to -6
722 °C, are the norm (Conen et al., 2011; Garcia et al., 2012; Hill et al., 2016; O’Sullivan et al., 2014).

Formatted: Font: Bold

Formatted: Font: Not Italic

723 ~~and the high activity of agricultural soil particles has been attributed to internally mixed organic~~
724 ~~matter (O'Sullivan et al., 2014; Tobo et al., 2014).~~

725 Organic material can condense or adsorb onto aerosols during photochemical and oxidative
726 processes, representing another potential source of organic INPs during AQABA (Dall'Osto et al.,
727 2010; Hinz et al., 2005; Krueger et al., 2004). Could aging explain the organics and decreased n_s
728 observed? Though dust aerosol was collected within 1 day's transport from source regions
729 throughout this study, we cannot rule out the possibility of aging impacts, lacking single particle
730 chemistry measurements (e.g., Sullivan et al., 2007). In addition to field observations of $n_{\text{INP_INP}}$
731 ~~concentrations~~ demonstrating that aging increased the IN efficiency of desert dust INPs (see
732 Introduction; Boose et al., 2016; Conen et al. 2015), prior studies of the effects of aging on mineral
733 dust INPs have yielded mixed and sometimes contradictory results, indicating that the impact of
734 aging on IN properties likely depends on multiple factors including the ice nucleation pathway,
735 the type of aging process, surface morphology, and mineralogy (Perkins et al., 2020 ~~and references~~
736 ~~therein~~). Multiple studies have investigated the effects of various aging processes on Arizona Test
737 Dust (ATD) as a proxy for diverse natural dust samples. These included exposure to sulfuric acid,
738 nitric acid vapor, and solution-phase processes (Cziczo et al., 2009; Eastwood et al., 2009; Knopf
739 and Koop, 2006; Salam et al., 2007; Sullivan et al., 2010b, 2010a). Perkins et al. (2020)
740 demonstrated the INP lability in ATD through multiple solution-phase aging processes (e.g.,
741 incubation in water, exposure to acid or salt), with up to 1000~~×-fold~~ reductions in INP abundance
742 at freezing temperatures > 10 °C. This result contrasts with the increase in IN activity attributed to
743 aging reported in Boose et al. (2016) and Conen et al. (2015). Perkins et al. (2020) additionally
744 reported that the lability of IN activity in ATD is temperature dependent, with large reductions
745 evident at freezing temperature > 10 °C, yet little to no change at temperatures ~~\leq below~~ -15 °C. By
746 contrast, most of the n_s spectra in AQABA samples were 10 – 1000 \times lower than established dust
747 parameterizations even at temperatures ~~\leq below~~ -15 °C. In summary, it has proven difficult to
748 determine any consistent impact of atmospheric processing on the IN activity of dust in model
749 systems such as ATD (Perkins et al., 2020), and few studies have investigated impacts of aging on
750 ambient desert dust, especially at modest supercooling (Boose et al., 2016). Furthermore, the use
751 of ATD as a proxy for natural dust in INP studies has been questioned due to the complex ~~ice-~~
752 ~~nucleating~~ ~~IN~~ properties of natural dust, including mineral composition and defect sites at the

Field Code Changed

753 particle surface, the latter of which is likely affected by the mechanical processing and milling
754 involved in ATD production (e.g., Perkins et al., 2020 and references therein).

755 ~~Gong et al. (2020) also observed n_s lower by more than 2 orders of magnitude compared to N12~~
756 ~~and U17 despite the large fraction of supermicron INPs (77-83% depending on temperature), and~~
757 ~~that the supermicron particles were mainly mineral dust. The large differences between~~
758 ~~parameterized n_s for dust, and n_s observed in both Gong et al. (2020) and the present study between~~
759 ~~-12 and -25 °C demonstrate that existing n_s -based parameterizations may not faithfully represent~~
760 ~~n_s at moderate freezing temperatures, despite proximity to major source regions. Whereas DeMott~~
761 ~~et al. (2015a) found that for temperatures < 20 °C, mineral dust particles from Saharan and Asian~~
762 ~~deserts may be parameterized as a common particle type, our findings suggest that characteristic~~
763 ~~n_s parameterizations for dust from different source regions may be needed > 20 °C, or,~~
764 ~~alternatively, that this temperature regime requires an alternative to an n_s -based parameterizations.~~
765 ~~Gong et al. (2019a) demonstrated that predicting n_{INP} from surface area size distributions alone~~
766 ~~may not be feasible in environments where the aerosol and/or INP composition are unknown and~~
767 ~~proposed a probability density function PDF-based approach to predicting INPs at a given freezing~~
768 ~~temperature.~~

769 Gong et al. (2020) also observed n_s lower by more than 2 orders of magnitude compared to N12
770 and U17 despite the large fraction of supermicron INPs (77-83% depending on temperature), and
771 that the supermicron particles were mainly mineral dust. The cause of the decreased n_s observed
772 here and in Gong et al. (2020) compared to dust n_s parameterizations remains elusive. Both studies
773 were conducted in air masses dominated by dust near major sources. In contrast, Price et al. (2018)
774 found agreement near the region of the Gong et al. (2020) study. One obvious difference is that
775 Price et al. (2018) conducted measurements at higher altitudes, between 30 and 3500 m. A prior
776 study that compared n_{INP} in dust-laden air masses at the surface with n_{INP} collected between 0.5
777 and 3 km above sea level found that median n_{INP} increased by up to 10× above the surface and
778 correlated to dust loading (Schrod et al., 2017). The differences between Price et al. (2018) and

Formatted: Font: Not Italic

Formatted: Font: Not Italic

Formatted: Font: Not Italic

779 the two surface-based studies draws attention to the need for vertical profiles of $n_s > -25$ °C in
780 dust-laden air masses.

781 The decreased n_s compared to Price et al. (2018) is also unlikely to be related to differences in INP
782 measurement. In all three studies, cold stage or droplet assay measurements of immersion mode
783 INPs were used in resuspensions of aerosol collected on filter samples. Recent studies that
784 intercompared instruments designed for measurement of immersion mode INPs showed excellent
785 agreement (i.e., within measurement uncertainty) in measurements of standardized dust and
786 biological samples (DeMott et al., 2018) and when co-sampling ambient aerosol (DeMott et al.,
787 2017). Moreover, the DeMott et al. (2018) intercomparison study demonstrated good agreement
788 in multiple natural dust samples between the various measurement methods used to derive D15,
789 N12 and U17 and the droplet assay methods applied in Gong et al. (2020), Price et al. (2018),
790 and the present study.

791 Storage protocol represents another difference between Price et al. (2018) and the two surface-
792 based studies. Gong et al. (2020) and the present study stored samples frozen prior to analysis,
793 whereas Price et al. (2018) processed samples immediately after collection. An understanding of
794 storage impacts on INPs collected on filters is lacking (Wex et al., 2019), but we note that the
795 discrepancies in n_s between the two surface-based studies and Price et al. (2018) exceed the range
796 of INP concentration changes reported in untreated INP precipitation samples stored frozen (Beall
797 et al., 2020).

798 Thus, the large differences between parameterized n_s for dust, and n_s observed in both Gong et al.
799 (2020) and the present study between -12 and -25 °C indicate that existing n_s -based
800 parameterizations may not faithfully represent n_s at moderate freezing temperatures, despite
801 proximity to major source regions. Whereas DeMott et al. (2015) found that for temperatures < -20
802 °C, mineral dust particles from Saharan and Asian deserts may be parameterized as a common
803 particle type, our findings suggest that characteristic n_s parameterizations for dust from different
804 source regions may be needed > -20 °C, or, alternatively, that this temperature regime requires an
805 alternative to an n_s -based parameterizations. Gong et al. (2019a) demonstrated that predicting n_{INP}
806 from surface area size distributions alone may not be feasible in environments where the aerosol
807 and/or INP composition are unknown and proposed a probability density function (PDF)-based

Formatted: No widow/orphan control, Don't keep with next

Formatted: Font: Not Italic

808 approach to predicting INPs at a given freezing temperature.

809 In light of the evidence from this study that INPs were primarily influenced by organics associated
810 with dust, especially at higher temperatures, and the lack of relationship between dust loading, n_s ,
811 and n_{INP} , we offer the following points for consideration. —Prior studies of aerosolized dust
812 demonstrated that it is frequently enriched in organic matter (6-20×) compared to soil dust and
813 that wind erosion selectively removes the chemically-enriched, fine portion of the soil higher ~~of~~
814 in plant nutrients, organic matter and metals (Aryal et al., 2012; Delany and Zenchelsky, 1976;
815 Van Pelt and Zobeck, 2007). Furthermore, a recent study that measured airborne concentrations of
816 prokaryotic cells over the Red Sea characterized the region as a “global hot spot” with average
817 concentrations of 155,000 (\pm 65,000) cells m⁻³, 19× higher than that over the subtropical and
818 tropical open oceans (Mayol et al., 2014; Yahya et al., 2019). Yahya et al. (2019) demonstrated
819 that the microbial loading was very likely related to the high concentrations of dust, as 99.9% of
820 the cells were attached to dust particles. Organic and biological species have been shown to
821 dominate IN activity at temperatures $> \sim -15$ °C in many studies (e.g., Kanji et al., 2017; Ladino et
822 al., 2019; O’Sullivan et al., 2018, Kanji et al., 2017, and references therein). Thus, a faithful
823 representation of dust INPs may require two parameterizations: one for the IN activity dominated
824 by minerals $< \sim -15$ °C such as D15, U17 and N12, and another for the dust-associated organics $>$
825 ~ -15 °C. As IN-active organics are limited compared to the IN-active mineral component of dust,
826 we could expect an increase in n_s slope between warm and cold regimes. The apparent decreased
827 n_s observed in this study between -18 and -12 °C could potentially be related to a plateau in n_s
828 through the transition between the mineral and organic “modes” (see untreated samples in Figs. 5-
829 Fig. 65). This study underscores the need to characterize the IN-active organic species associated
830 with dust from major source regions and to investigate the extent to which biological and/or
831 organic particles contribute to INP populations in dust-laden air masses at high to moderate
832 freezing temperatures ≥ -15 °C.

833 **3.2 Seawater Source Potential**

834 ~~The n_{INP} values in 10 SSW samples collected during AQABA were used to characterize the INP~~
835 ~~source potential of SSA generated by bubble bursting (Wang et al., 2017). Results from prior~~
836 ~~studies have demonstrated that jet droplets are a more efficient transfer vehicle than film drops of~~

Formatted: Font: Not Italic

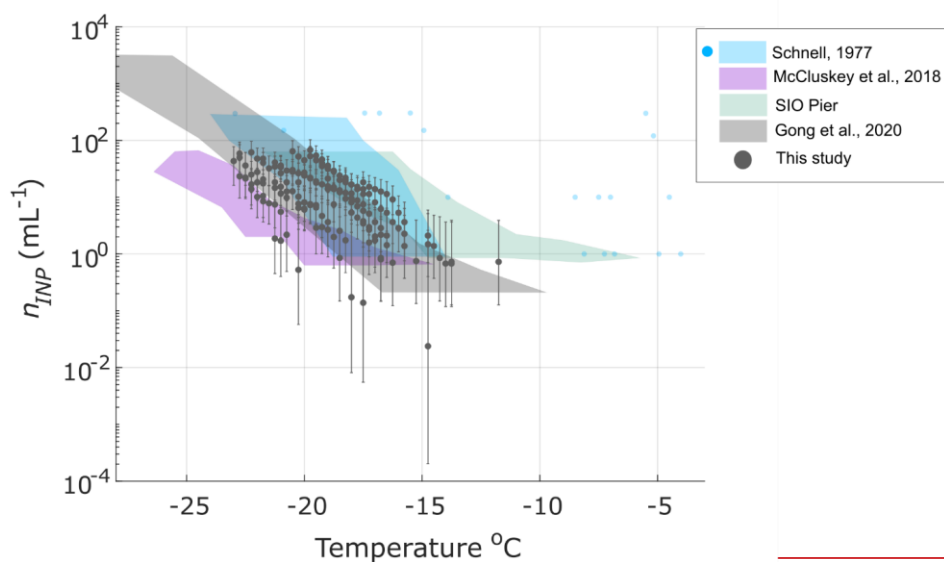
Formatted: Superscript

Formatted: Justified

837 INPs into SSA particles (Mitts et al., 2021; Wang et al., 2017). While it is unlikely that many of
838 the INPs detected in aerosol samples were marine in origin (see Sec. 3.1), we measured the INP
839 concentrations in SSW to test whether the seawater source strength was comparable to that of prior
840 studies, or were possibly enriched with INPs due to biological activity or even dust deposition
841 (Cornwell et al., 2020).

842 Figure S10 shows how the INP concentrations measured at -19°C in 10 seawater samples varied
843 by the sample collection location. Concentrations ranged between 1 and 50 INPs mL^{-1} and were
844 highest between the Gulf of Oman and the Gulf of Aden. This region exhibited relatively high
845 chlorophyll a during the cruise, with levels between 1 and 30 mg m^{-3} (Fig. S11). In Fig. 6, INP
846 concentrations were compared with SSW from the Ellen Browning Scripps Memorial Pier in
847 coastal Southern California (SIO Pier), Cabo Verde in the Northeast Atlantic, the Southern
848 Ocean (McCluskey et al., 2017), and the Northwest Atlantic (Schnell, 1977). AQABA INP
849 concentrations were most comparable with Gong et al.'s (2020) observations in Cabo Verde. The

850 lack of any unusually high INP spectra suggests that INP enrichment due to dust deposition
851 (Cornwell et al. 2020) was absent or infrequent.



852
853 **Figure 6.** Measured INP concentrations in 10 SSW samples collected during AQABA. Also
854 shown are the composite INP spectrum of coastal SSW samples collected on São Vicente
855 Island, Cabo Verde (Gong et al., 2020), coastal SSW samples collected at the Ellen Browning
856 Scripps Pier (green shading), and SSW samples collected in the Southern Ocean (McCluskey et
857 al., 2018d). Schnell's (1977) SSW measurements are represented as a composite spectrum of 24
858 samples (blue shaded region) and 5 additional spectra (blue markers) from samples that exhibited
859 higher freezing temperatures. All spectra presented are uncorrected for freezing point depression.
860 ~~Offline treatments for testing heat lability, organic composition, and size were applied to 5 of the~~
861 ~~10 seawater samples (Methods Sec. 2.4). Heat and 0.2 μm filtering treatments suggest that a~~
862 ~~large fraction of the seawater INPs were heat sensitive and larger than 0.2 μm. These results are~~
863 ~~indicative of the particulate organic carbon (POC) type of marine INP defined in McCluskey et~~
864 ~~al. (2018a) (Fig. S12).~~

Formatted: Font: (Default) Times New Roman, 12 pt

865 ~~Heat resilience but peroxide sensitivity in sample s001 additionally indicates the presence of~~
866 ~~non-proteinaceous organic INPs, such as the dissolved organic carbon (DOC) type defined in~~
867 ~~McCluskey et al. (2018a). Considering the characteristically low IN activity of the SSW, the~~
868 ~~lower n_s of SSA compared to mineral dust (McCluskey et al., 2018b), and the frequency of dust~~
869 ~~events during AQABA, our findings suggest that dust was highly likely to be the dominant INP~~
870 ~~class observed in this study.~~

871

872 **5.4 Conclusions**

873 Observations from the two-month AQABA campaign in the Mediterranean, Red Sea, Arabian Sea
874 and Arabian Gulf are among the first INP measurements made in close proximity to the two largest
875 dust sources globally: the Sahara and the Arabian Peninsula (Kok et al., 2021). ~~Observed n_{INP} INP~~
876 ~~concentrations measured in 26 aerosol samples~~ spanned ~~two-2 or more~~ orders of magnitude (~~$5 \times$~~
877 ~~10^{-3} to $5 \times 10^{-1} \text{ L}^{-1}$~~ ~~$0.002$ to 0.5 L^{-1}~~ at -15°C).

878 In summary, INPs observed during AQABA were very likely dominated by mineral dust with
879 some additional contributions possibly from densely-populated and/or agricultural regions
880 including the Nile River Delta region and Southern or Eastern Europe. Despite proximity to major
881 dust sources and a high frequency of dust events with ~~MERRA-2 simulated~~ mass concentrations
882 up to $490 \mu\text{g m}^{-3}$ (PM_{10}), the observed n_s for most samples was lower by 1-3 orders of magnitude
883 compared to n_s predicted by dust parametrizations N12 and U17 at $T < -12^\circ\text{C}$ (~~Niemand et al.,~~
884 ~~2012; Ullrich et al., 2017~~). ~~Observed n_s for some samples was equivalent to that of Many INPs~~
885 ~~measured in AQABA showed agreement with~~ the A13 parameterization for K-feldspar (Atkinson
886 et al., 2013), an ice-active component of desert dust, ~~with~~ observations within the marine boundary
887 layer (DeMott et al., 2016; Yang et al., 2020), and ~~with the~~ Price et al.'s (2018) measurements of
888 ~~n_{INP} INP concentrations~~ in dust-laden air masses over the Tropical Atlantic. Peroxide sensitivity
889 was evident in all samples tested (12 of 26), at temperatures $\geq -15^\circ\text{C}$, demonstrating a consistent
890 contribution of organic material to warm-temperature INPs. Heat-sensitivity further suggested the
891 presence of biological (e.g., proteinaceous) INPs in a subset of samples, particularly at high
892 freezing temperatures $> -10^\circ\text{C}$. ~~While the dominant mineral dusts in the region are associated with~~
893 ~~the lowest concentrations of soil organic carbon globally (e.g., Yost and Hartemink, 2019 and~~

Formatted: Font: Italic

Formatted: Subscript

Formatted: Font: Not Bold

Formatted: Font: Not Bold

Formatted: Font: Not Bold

Formatted: Font: Not Bold

894 ~~references therein), aerosolized fine dust is known to be enriched in organic matter (Aryal et al.,~~
895 ~~2012; Delany and Zenehelsky, 1976; Van Pelt and Zobeck, 2007) and is additionally associated~~
896 ~~with high microbial loading in the Red Sea (Yahya et al., 2019).~~ A soil dust sample from North
897 Africa (~~originally from N12~~) exhibited heat and peroxide sensitivity between -5 and -16 °C, further
898 demonstrating that the IN activity of mineral dust could be associated with organic and/or
899 biological material. Contrary to Price et al. (2018), who measured INP in the dust-laden Tropical
900 Atlantic, no correlation was found between dust loading and n_{INP} or n_s . Results from this study and
901 Gong et al. (2020) indicate that the existing n_s parameterizations alone do not skillfully represent
902 mineral dust associated INPs at modest supercooling near major dust sources.

Formatted: Font: Not Italic

903 The source strengths of Red Sea, Mediterranean, Arabian Sea, and Arabian Gulf bulk seawater
904 were also evaluated. The maximum source potential was observed in the Arabian Sea (50 INP
905 mL^{-1} at -19 °C.) ~~Overall, the~~The observed n_{INP} ~~range for SSW samples were equivalent to agreed~~
906 ~~well with the those of~~ Gong et al. (2020) ~~SSW measurements~~ at Cabo Verde ~~within the 95%~~
907 ~~binomial sampling confidence intervals (Agresti and Coull, 1998).~~

Formatted: Font: Not Italic

Formatted: Font: Not Bold

908 Considering that desert dust parameterizations overpredicted the n_s values observed during
909 AQABA, despite proximity to major global emissions sources, this study demonstrates the need
910 to evaluate the fidelity of dust INP parameterizations in nascent versus aged dust populations.

Formatted: Line spacing: 1.5 lines

911 The discrepancies underscore the challenges of evaluating dust-specific INP parameterizations:
912 limited observations at modest supercooling, few assured methods for distinguishing between
913 different INP sources in ambient aerosol, a dearth of characteristic soil dust samples from major
914 dust sources, and limited knowledge of the specific composition and characteristics of dust INPs
915 at temperatures > -15 °C. ~~Vertical profiles of n_s in dust-laden air masses are also needed to~~
916 ~~determine whether n_s is consistently lower at the surface and examine the variability of n_s with~~
917 ~~altitude. Potential storage impacts on INPs collected on filters are an additional factor worthy of~~
918 ~~future investigation, though storage alone does not likely explain the relatively decreased n_s~~
919 ~~compared to parameterizations observed in this study, as U17 and N12 were both derived from~~
920 ~~stored dust samples.~~

Formatted: Font: (Default) Times New Roman, 12 pt

Formatted: Font: (Default) Times New Roman, 12 pt

Formatted: Font: (Default) Times New Roman, 12 pt

Formatted: Font: (Default) Times New Roman, 12 pt

921

922 In addition to providing observations at high to moderate freezing temperatures, future studies
923 could apply the methods developed in Gong et al. (2020) to estimate the contribution of marine
924 INPs to the aerosol sampled by assuming equivalent distributions of sea salt and INPs between
925 seawater and air. Furthermore, given the combination of marine, dust, and anthropogenically-
926 influenced air masses encountered, and the evidence of organic and biological INPs at modest
927 supercooling in this study and Gong et al. (2020), future studies could benefit from advances in
928 on-line Light-Induced Fluorescence (LIF) measurement techniques. Whereas the interpretation of
929 fluorescence data from most LIF-based instruments has been limited by the lack of spectroscopic
930 information, newer instruments support real-time spectrally-resolved size and fluorescence
931 measurement information for single particles (Fennelly et al., 2018; Huffman et al., 2020;
932 Könemann et al., 2019). This information could be used to potentially “tag” different classes of
933 organics and biological aerosols, enabling investigations of relationships between n_s , n_{INP} and
934 organic signatures in, e.g., mineral dusts and agricultural soil dusts. Finally, the decreased n_s
935 observed in this study further motivate comprehensive aerosol-ice nucleation studies, which aim
936 to achieve closure between measured and predicted ambient ~~n_{INP} concentrations~~ by
937 simultaneously characterizing ambient INPs and ice nucleation relevant properties of the total
938 aerosol population, such as composition and aerosol chemical mixing state (Sullivan et al., 2007).

939 **Data Availability:** The data set supporting this manuscript is hosted by the UCSD Library
940 Digital Collections (<https://doi.org/10.6075/J0X0676P>) (Beall et al., 2021).

941 **Author contributions:**

942 CMB, TCH, PJD, MOA, CP, JL, JS, FD, BW, HH, MDS, and KAP designed the study. CMB
943 performed the INP measurements, FLEXPART modeling and analysis with support from TCH,
944 PJD, MOA, MDS, MP and KAP. TCH, PJD and MOA contributed significantly to the writing,
945 preparation of figures and analysis. TK, MI, RP and HH supported the field collection of aerosol
946 for INP analysis and TK additionally provided aerosol number concentration data. JS and MP

Formatted: Font: Not Italic

Formatted: Font: 12 pt

Formatted: Font: 12 pt

Formatted: Font: 12 pt

947 provided aerosol water-soluble composition data. FD oversaw the aerosol sizing and AMS
948 composition measurements and analysis. All authors contributed to the writing of the article.

949 **Competing interests:**

950 The authors declare they have no conflict of interest.

951

952 **Acknowledgements:**

953 The authors acknowledge collaborations with King Abdullah University of Science and
954 Technology (KAUST), the Cyprus Institute (CyI) and the Kuwait Institute for Scientific
955 Research (KISR). We additionally thank Marcel Dorf and Claus Koeppel for the organization of
956 the campaign, as well as Horst Fischer, Ivan Tadic and Uwe Parchatka for provision of the NO
957 data. Analyses and visualizations of dust mass concentrations and Chl *a* used in this paper were
958 produced with the Giovanni online data system, developed and maintained by the NASA GES
959 DISC. Maps throughout this article were created using ArcGIS® software by Esri. We would
960 also like to thank Hays Ships Ltd. and the *Kommandor Iona*'s crew for their attention to the
961 safety and well-being of the researchers. Finally, we thank the three anonymous reviewers whose
962 insightful comments strengthened this paper. Funding was provided by Highly Cited Program at
963 King Saud University and the Max Planck Society and the University of California San Diego
964 (UCSD) Understanding and Protecting the Planet initiative.

965

966

967 **References**

968 Agresti, A. and Coull, B. A.: Approximate Is Better than "Exact" for Interval Estimation of Binomial
969 Proportions, *Am. Stat.*, 52(2), 119, doi:10.2307/2685469, 1998.

970 Ardon-Dryer, K. and Levin, Z.: Ground-based measurements of immersion freezing in the eastern
971 Mediterranean, *Atmos. Chem. Phys.*, 14(10), 5217–5231, doi:10.5194/acp-14-5217-2014, 2014.

972 Aryal, R., Kandel, D., Acharya, D., Chong, M. N. and Beecham, S.: Unusual Sydney dust storm and its
973 mineralogical and organic characteristics, *Environ. Chem.*, 9(6), 537–546 [online] Available from:

Formatted: Font: 12 pt

Formatted: Font: (Default) Times New Roman, 12 pt

974 <https://doi.org/10.1071/EN12131>, 2012.

975 Atkinson, J. D., Murray, B. J., Woodhouse, M. T., Whale, T. F., Baustian, K. J., Carslaw, K. S., Dobbie,
976 S., O'Sullivan, D. and Malkin, T. L.: The importance of feldspar for ice nucleation by mineral dust in
977 mixed-phase clouds, *Nature*, 498(7454), 355–358, doi:10.1038/nature12278, 2013.

978 Beall, C. M., Stokes, M. D., Hill, T. C., DeMott, P. J., DeWald, J. T. and Prather, K. A.: Automation and
979 Heat Transfer Characterization of Immersion Mode Spectroscopy for Analysis of Ice Nucleating
980 Particles, *Atmos. Meas. Tech.*, (February), 1–25, doi:10.5194/amt-2016-412, 2017.

981 Beall, C. M., Lucero, D., Hill, T. C., DeMott, P. J., Stokes, M. D. and Prather, K. A.: Best practices for
982 precipitation sample storage for offline studies of ice nucleation in marine and coastal environments,
983 *Atmos. Meas. Tech.*, 13(12), 6473–6486, doi:10.5194/amt-13-6473-2020, 2020.

984 Beall, C. M., Michaud, J. M., Fish, M. A., Dinasquet, J., Cornwell, G. C., Stokes, M. D., Burkart, M. D.,
985 Hill, T. C., Demott, P. J. and Prather, K. A.: Cultivable halotolerant ice-nucleating bacteria and fungi in
986 coastal precipitation, *Atmos. Chem. Phys.*, 21(11), 9031–9045, doi:10.5194/acp-21-9031-2021, 2021.

987 Boose, Y., Sierau, B., Isabel García, M., Rodríguez, S., Alastuey, A., Linke, C., Schnaiter, M.,
988 Kupiszewski, P., Kanji, Z. A. and Lohmann, U.: Ice nucleating particles in the Saharan Air Layer, *Atmos.*
989 *Chem. Phys.*, 16(14), 9067–9087, doi:10.5194/acp-16-9067-2016, 2016.

990 Boose, Y., Baloh, P., Plötze, M., Ofner, J., Grothe, H., Sierau, B., Lohmann, U. and Kanji, Z. A.:
991 Heterogeneous ice nucleation on dust particles sourced from nine deserts worldwide -- Part 2: Deposition
992 nucleation and condensation freezing, *Atmos. Chem. Phys.*, 19(2), 1059–1076, doi:10.5194/acp-19-1059-
993 2019, 2019.

994 Bourtsoukidis, E., Ernle, L., Crowley, J. N., Lelieveld, J., Paris, J.-D., Pozzer, A., Walter, D. and
995 Williams, J.: Non-methane hydrocarbon (C_2 – C_8) sources and sinks around the
996 Arabian Peninsula, *Atmos. Chem. Phys.*, 19(10), 7209–7232, doi:10.5194/acp-19-7209-2019, 2019.

997 Bourtsoukidis, E., Pozzer, A., Sattler, T., Matthaios, V. N., Ernle, L., Edtbauer, A., Fischer, H.,
998 Könemann, T., Osipov, S., Paris, J.-D., Pfannerstill, E. Y., Stönnner, C., Tadic, I., Walter, D., Wang, N.,
999 Lelieveld, J. and Williams, J.: The Red Sea Deep Water is a potent source of atmospheric ethane and
1000 propane, *Nat. Commun.*, 11(1), 447, doi:10.1038/s41467-020-14375-0, 2020.

1001 Broadley, S. L., Murray, B. J., Herbert, R. J., Atkinson, J. D., Dobbie, S., Malkin, T. L., Condliffe, E. and
1002 Neve, L.: Immersion mode heterogeneous ice nucleation by an illite rich powder representative of
1003 atmospheric mineral dust, *Atmos. Chem. Phys.*, 12(1), 287–307, doi:10.5194/acp-12-287-2012, 2012.

1004 Brunner, C., Brem, B. T., Collaud Coen, M., Conen, F., Hervo, M., Henne, S., Steinbacher, M., Gysel-
1005 Beer, M. and Kanji, Z. A.: The contribution of Saharan dust to the ice-nucleating particle concentrations
1006 at the High Altitude Station Jungfraujoch (3580\,m\,a.s.l.), Switzerland, *Atmos. Chem. Phys.*, 21(23),
1007 18029–18053, doi:10.5194/acp-21-18029-2021, 2021.

1008 Buchard, V., Randles, C. A., da Silva, A. M., Darmenov, A., Colarco, P. R., Govindaraju, R., Ferrare, R.,
1009 Hair, J., Beyersdorf, A. J., Ziemba, L. D. and Yu, H.: The MERRA-2 Aerosol Reanalysis, 1980 Onward.
1010 Part II: Evaluation and Case Studies, *J. Clim.*, 30(17), 6851–6872, doi:10.1175/JCLI-D-16-0613.1, 2017.

1011 Burrows, S. M., Hoose, C., Pöschl, U. and Lawrence, M. G.: Ice nuclei in marine air: biogenic particles or
1012 dust?, *Atmos. Chem. Phys.*, 13(1), 245–267, doi:10.5194/acp-13-245-2013, 2013.

1013 Celik, S., Drewnick, F., Fachinger, F., Brooks, J., Darbyshire, E., Coe, H., Paris, J.-D., Eger, P. G.,
1014 Schuladen, J., Tadic, I., Friedrich, N., Dienhart, D., Hottmann, B., Fischer, H., Crowley, J. N., Harder, H.
1015 and Borrmann, S.: Influence of vessel characteristics and atmospheric processes on the gas and particle
1016 phase of ship emission plumes: in situ measurements in the Mediterranean Sea and around the Arabian
1017 Peninsula, *Atmos. Chem. Phys.*, 20(8), 4713–4734, doi:10.5194/acp-20-4713-2020, 2020.

1018 Collins, D. B., Zhao, D. F., Ruppel, M. J., Laskina, O., Grandquist, J. R., Modini, R. L., Stokes, M. D.,
1019 Russell, L. M., Bertram, T. H., Grassian, V. H., Deane, G. B. and Prather, K. A.: Direct aerosol chemical
1020 composition measurements to evaluate the physicochemical differences between controlled sea spray
1021 aerosol generation schemes, *Atmos. Meas. Tech.*, 7(11), 3667–3683, doi:10.5194/amt-7-3667-2014,
1022 2014.

1023 Conen, F., Morris, C. E., Leifeld, J., Yakutin, M. V and Alewell, C.: Biological residues define the ice
1024 nucleation properties of soil dust, *Atmos. Chem. Phys.*, 11(18), 9643–9648, doi:10.5194/acp-11-9643-
1025 2011, 2011.

1026 Conen, F., Rodríguez, S., Hüglin, C., Henne, S., Herrmann, E., Bukowiecki, N. and Alewell, C.:
1027 Atmospheric ice nuclei at the high-altitude observatory Jungfraujoch, Switzerland, *Tellus, Ser. B Chem.*
1028 *Phys. Meteorol.*, 67(1), 1–10, doi:10.3402/tellusb.v67.25014, 2015.

1029 Conen, F., Einbock, A., Mignani, C. and Hüglin, C.: Measurement report: Ice-nucleating particles active
1030 $\geq -15^{\circ}\text{C}$ in free tropospheric air over western Europe, *Atmos. Chem. Phys.*, 22(5), 3433–
1031 3444, doi:10.5194/acp-22-3433-2022, 2022.

1032 Cornwell, G. C., McCluskey, C. S., Levin, E. J. T., Suski, K. J., DeMott, P. J., Kreidenweis, S. M. and
1033 Prather, K. A.: Direct Online Mass Spectrometry Measurements of Ice Nucleating Particles at a California
1034 Coastal Site, *J. Geophys. Res. Atmos.*, 124(22), 12157–12172, doi:doi:10.1029/2019JD030466, 2019.

1035 Cornwell, G. C., Sultana, C. M., Prank, M., Cochran, R. E., Hill, T. C. J., Schill, G. P., DeMott, P. J.,
1036 Mahowald, N. and Prather, K. A.: Ejection of Dust From the Ocean as a Potential Source of Marine Ice
1037 Nucleating Particles, *J. Geophys. Res. Atmos.*, 125(24), e2020JD033073,
1038 doi:<https://doi.org/10.1029/2020JD033073>, 2020.

1039 Cziczo, D. J., Froyd, K. D., Gallavardin, S. J., Moehler, O., Benz, S., Saathoff, H. and Murphy, D. M.:
1040 Deactivation of ice nuclei due to atmospherically relevant surface coatings, *Environ. Res. Lett.*, 4(4),
1041 44013, doi:10.1088/1748-9326/4/4/044013, 2009.

1042 Dall'Osto, M., Harrison, R. M., Highwood, E. J., O'Dowd, C., Ceburnis, D., Querol, X. and Achterberg,
1043 E. P.: Variation of the mixing state of Saharan dust particles with atmospheric transport, *Atmos. Environ.*,
1044 44(26), 3135–3146, doi:<https://doi.org/10.1016/j.atmosenv.2010.05.030>, 2010.

1045 Delany, A. C. and Zenchelsky, S.: THE ORGANIC COMPONENT OF WIND-EROSION-
1046 GENERATED SOIL-DERIVED AEROSOL, *Soil Sci.*, 121(3) [online] Available from:
1047 [https://journals.lww.com/soilsci/Fulltext/1976/03000/THE_ORGANIC_COMPONENT_OF_WIND_ER](https://journals.lww.com/soilsci/Fulltext/1976/03000/THE_ORGANIC_COMPONENT_OF_WIND_EROSION_GENERATED.2.aspx)
1048 [OSION_GENERATED.2.aspx](https://journals.lww.com/soilsci/Fulltext/1976/03000/THE_ORGANIC_COMPONENT_OF_WIND_EROSION_GENERATED.2.aspx), 1976.

1049 Demott, P. J., Prenni, A. J., Mcmeeking, G. R., Sullivan, R. C., Petters, M. D., Tobo, Y., Niemand, M.,
1050 Möhler, O., Snider, J. R., Wang, Z. and Kreiden: Integrating laboratory and field data to quantify the
1051 immersion freezing ice nucleation activity of mineral dust particles, , 393–409, doi:10.5194/acp-15-393-
1052 2015, 2015.

1053 DeMott, P. J., Hill, T. C. J., McCluskey, C. S., Prather, K. A., Collins, D. B., Sullivan, R. C., Ruppel, M.
1054 J., Mason, R. H., Irish, V. E., Lee, T., Hwang, C. Y., Rhee, T. S., Snider, J. R., McMeeking, G. R.,
1055 Dhaniyala, S., Lewis, E. R., Wentzell, J. J. B., Abbatt, J., Lee, C., Sultana, C. M., Ault, A. P., Axson, J.
1056 L., Diaz Martinez, M., Venero, I., Santos-Figueroa, G., Stokes, M. D., Deane, G. B., Mayol-Bracero, O.
1057 L., Grassian, V. H., Bertram, T. H., Bertram, A. K., Moffett, B. F. and Franc, G. D.: Sea spray aerosol as
1058 a unique source of ice nucleating particles, *Proc. Natl. Acad. Sci.*, 113(21), 5797–5803,
1059 doi:10.1073/pnas.1514034112, 2016.

1060 DeMott, P. J., Hill, T. C. J., Petters, M. D., Bertram, A. K., Tobo, Y., Mason, R. H., Suski, K. J.,
1061 McCluskey, C. S., Levin, E. J. T., Schill, G. P., Boose, Y., Rauker, A. M., Miller, A. J., Zaragoza, J.,
1062 Rocci, K., Rothfuss, N. E., Taylor, H. P., Hader, J. D., Chou, C., Huffman, J. A., Pöschl, U., Prenni, A. J.
1063 and Kreidenweis, S. M.: Comparative measurements of ambient atmospheric concentrations of ice
1064 nucleating particles using multiple immersion freezing methods and a continuous flow diffusion chamber,
1065 *Atmos. Chem. Phys.*, 17(18), 11227–11245, doi:10.5194/acp-17-11227-2017, 2017.

1066 DeMott, P. J., Möhler, O., Cziczo, D. J., Hiranuma, N., Petters, M. D., Petters, S. S., Belosi, F.,
1067 Bingemer, H. G., Brooks, S. D., Budke, C., Burkert-Kohn, M., Collier, K. N., Danielczok, A., Eppers, O.,
1068 Felgitsch, L., Garimella, S., Grothe, H., Herenz, P., Hill, T. C. J., Höhler, K., Kanji, Z. A., Kiselev, A.,
1069 Koop, T., Kristensen, T. B., Krüger, K., Kulkarni, G., Levin, E. J. T., Murray, B. J., Nicosia, A.,
1070 O'Sullivan, D., Peckhaus, A., Polen, M. J., Price, H. C., Reicher, N., Rothenberg, D. A., Rudich, Y.,
1071 Santachiara, G., Schiebel, T., Schrod, J., Seifried, T. M., Stratmann, F., Sullivan, R. C., Suski, K. J.,
1072 Szakáll, M., Taylor, H. P., Ullrich, R., Vergara-Temprado, J., Wagner, R., Whale, T. F., Weber, D., Welti,
1073 A., Wilson, T. W., Wolf, M. J. and Zenker, J.: The Fifth International Workshop on Ice Nucleation phase
1074 2 (FIN-02): laboratory intercomparison of ice nucleation measurements, *Atmos. Meas. Tech.*, 11(11),
1075 6231–6257, doi:10.5194/amt-11-6231-2018, 2018.

1076 Eastwood, M. L., Cremel, S., Wheeler, M., Murray, B. J., Girard, E. and Bertram, A. K.: Effects of
1077 sulfuric acid and ammonium sulfate coatings on the ice nucleation properties of kaolinite particles,
1078 *Geophys. Res. Lett.*, 36(2), doi:https://doi.org/10.1029/2008GL035997, 2009.

1079 Edtbauer, A., Stöner, C., Pfannerstill, E. Y., Berasategui, M., Walter, D., Crowley, J. N., Lelieveld, J.
1080 and Williams, J.: A new marine biogenic emission: methane sulfonamide (MSAM), dimethyl sulfide
1081 (DMS), and dimethyl sulfone (DMSO_2) measured in air over the Arabian Sea, *Atmos. Chem.*
1082 *Phys.*, 20(10), 6081–6094, doi:10.5194/acp-20-6081-2020, 2020.

1083 Eger, P. G., Friedrich, N., Schuladen, J., Shenolikar, J., Fischer, H., Tadic, I., Harder, H., Martinez, M.,
1084 Rohloff, R., Tauer, S., Drewnick, F., Fachinger, F., Brooks, J., Darbyshire, E., Sciare, J., Pikridas, M.,
1085 Lelieveld, J. and Crowley, J. N.: Shipborne measurements of ClNO_2 in the Mediterranean Sea and
1086 around the Arabian Peninsula during summer, *Atmos. Chem. Phys.*, 19(19), 12121–12140,
1087 doi:10.5194/acp-19-12121-2019, 2019.

1088 Fennelly, M. J., Sewell, G., Prentice, M. B., O'Connor, D. J. and Sodeau, J. R.: Review: The Use of Real-
1089 Time Fluorescence Instrumentation to Monitor Ambient Primary Biological Aerosol Particles (PBAP),
1090 *Atmosphere (Basel)*, 9(1), doi:10.3390/atmos9010001, 2018.

1091 Friedrich, N., Eger, P., Shenolikar, J., Sobanski, N., Schuladen, J., Dienhart, D., Hottmann, B., Tadic, I.,
1092 Fischer, H., Martinez, M., Rohloff, R., Tauer, S., Harder, H., Pfannerstill, E. Y., Wang, N., Williams, J.,
1093 Brooks, J., Drewnick, F., Su, H., Li, G., Cheng, Y., Lelieveld, J. and Crowley, J. N.: Reactive nitrogen
1094 around the Arabian Peninsula and in the Mediterranean Sea during the 2017 AQABA ship campaign,
1095 *Atmos. Chem. Phys.*, 21(10), 7473–7498, doi:10.5194/acp-21-7473-2021, 2021.

1096 Gandham, H., Dasari, H. P., Langodan, S., Karumuri, R. K. and Hoteit, I.: Major Changes in Extreme

1097 Dust Events Dynamics Over the Arabian Peninsula During 2003–2017 Driven by Atmospheric
1098 Conditions, *J. Geophys. Res. Atmos.*, 125(24), e2020JD032931,
1099 doi:<https://doi.org/10.1029/2020JD032931>, 2020.

1100 Gelaro, R., McCarty, W., Suárez, M. J., Todling, R., Molod, A., Takacs, L., Randles, C. A., Darmenov,
1101 A., Bosilovich, M. G., Reichle, R., Wargan, K., Coy, L., Cullather, R., Draper, C., Akella, S., Buchard,
1102 V., Conaty, A., da Silva, A. M., Gu, W., Kim, G.-K., Koster, R., Lucchesi, R., Merkova, D., Nielsen, J.
1103 E., Partyka, G., Pawson, S., Putman, W., Rienecker, M., Schubert, S. D., Sienkiewicz, M. and Zhao, B.:
1104 The Modern-Era Retrospective Analysis for Research and Applications, Version 2 (MERRA-2), *J. Clim.*,
1105 30(14), 5419–5454, doi:10.1175/JCLI-D-16-0758.1, 2017.

1106 Gong, X., Wex, H., Müller, T., Wiedensohler, A., Höhler, K., Kandler, K., Ma, N., Dietel, B., Schiebel,
1107 T., Möhler, O. and Stratmann, F.: Characterization of aerosol properties at Cyprus, focusing on cloud
1108 condensation nuclei and ice-nucleating particles, *Atmos. Chem. Phys.*, 19(16), 10883–10900,
1109 doi:10.5194/acp-19-10883-2019, 2019a.

1110 Gong, X., Wex, H., van Pinxteren, M., Triesch, N., Fomba, K. W., Lubitz, J., Stolle, C., Robinson, T.-B.,
1111 Müller, T., Herrmann, H. and Stratmann, F.: Ice nucleating particles measured in air, cloud and seawater
1112 at the Cape Verde Atmospheric Observatory (CVAO), , doi:10.1594/PANGAEA.906946, 2019b.

1113 Gong, X., Wex, H., van Pinxteren, M., Triesch, N., Fomba, K. W., Lubitz, J., Stolle, C., Robinson, T.-B.,
1114 Müller, T., Herrmann, H. and Stratmann, F.: Characterization of aerosol particles at Cabo Verde close to
1115 sea level and at the cloud level -- Part 2: Ice-nucleating particles in air, cloud and seawater, *Atmos. Chem.*
1116 *Phys.*, 20(3), 1451–1468, doi:10.5194/acp-20-1451-2020, 2020.

1117 Hara, K., Maki, T., Kakikawa, M., Kobayashi, F. and Matsuki, A.: Effects of different temperature
1118 treatments on biological ice nuclei in snow samples, *Atmos. Environ.*, 140, 415–419,
1119 doi:10.1016/j.atmosenv.2016.06.011, 2016.

1120 Harrison, A. D., Whale, T. F., Carpenter, M. A., Holden, M. A., Neve, L., O’Sullivan, D., Vergara
1121 Temprado, J. and Murray, B. J.: Not all feldspars are equal: a survey of ice nucleating properties across
1122 the feldspar group of minerals, *Atmos. Chem. Phys.*, 16(17), 10927–10940, doi:10.5194/acp-16-10927-
1123 2016, 2016.

1124 Harrison, A. D., Lever, K., Sanchez-Marroquin, A., Holden, M. A., Whale, T. F., Tarn, M. D., McQuaid,
1125 J. B. and Murray, B. J.: The ice-nucleating ability of quartz immersed in water and its atmospheric
1126 importance compared to K-feldspar, *Atmos. Chem. Phys.*, 19(17), 11343–11361, doi:10.5194/acp-19-
1127 11343-2019, 2019.

1128 Hartmann, M., Adachi, K., Eppers, O., Haas, C., Herber, A., Holzinger, R., Hünerbein, A., Jäkel, E.,
 1129 Jentzsch, C., van Pinxteren, M., Wex, H., Willmes, S. and Stratmann, F.: Wintertime Airborne
 1130 Measurements of Ice Nucleating Particles in the High Arctic: A Hint to a Marine, Biogenic Source for Ice
 1131 Nucleating Particles, *Geophys. Res. Lett.*, 47(13), e2020GL087770,
 1132 doi:<https://doi.org/10.1029/2020GL087770>, 2020.

1133 Hill, T. C. J., DeMott, P. J., Tobo, Y., Fröhlich-Nowoisky, J., Moffett, B. F., Franc, G. D. and
 1134 Kreidenweis, S. M.: Sources of organic ice nucleating particles in soils, *Atmos. Chem. Phys.*, 16(11),
 1135 7195–7211, doi:10.5194/acp-16-7195-2016, 2016.

1136 Hinz, K.-P., Trimborn, A., Weingartner, E., Henning, S., Baltensperger, U. and Spengler, B.: Aerosol
 1137 single particle composition at the Jungfraujoch, *J. Aerosol Sci.*, 36(1), 123–145,
 1138 doi:<https://doi.org/10.1016/j.jaerosci.2004.08.001>, 2005.

1139 Hiranuma, N., Augustin-Bauditz, S., Bingemer, H., Budke, C., Curtius, J., Danielczok, A., Diehl, K.,
 1140 Dreischmeier, K., Ebert, M., Frank, F., Hoffmann, N., Kandler, K., Kiselev, A., Koop, T., Leisner, T.,
 1141 Möhler, O., Nillius, B., Peckhaus, A., Rose, D., Weinbruch, S., Wex, H., Boose, Y., DeMott, P. J., Hader,
 1142 J. D., Hill, T. C. J., Kanji, Z. A., Kulkarni, G., Levin, E. J. T., McCluskey, C. S., Murakami, M., Murray,
 1143 B. J., Niedermeier, D., Petters, M. D., O’Sullivan, D., Saito, A., Schill, G. P., Tajiri, T., Tolbert, M. A.,
 1144 Welti, A., Whale, T. F., Wright, T. P. and Yamashita, K.: A comprehensive laboratory study on the
 1145 immersion freezing behavior of illite NX particles: a comparison of 17 ice nucleation measurement
 1146 techniques, *Atmos. Chem. Phys.*, 15(5), 2489–2518, doi:10.5194/acp-15-2489-2015, 2015.

1147 Hoose, C. and Möhler, O.: Heterogeneous ice nucleation on atmospheric aerosols: A review of results
 1148 from laboratory experiments., 2012.

1149 Hoose, C., Kristjánsson, J. E., Chen, J.-P. and Hazra, A.: A Classical-Theory-Based Parameterization of
 1150 Heterogeneous Ice Nucleation by Mineral Dust, Soot, and Biological Particles in a Global Climate Model,
 1151 *J. Atmos. Sci.*, 67(8), 2483–2503, doi:10.1175/2010JAS3425.1, 2010.

1152 Huffman, J. A., Perring, A. E., Savage, N. J., Clot, B., Crouzy, B., Tummon, F., Shoshanim, O., Damit,
 1153 B., Schneider, J., Sivaprakasam, V., Zawadowicz, M. A., Crawford, I., Gallagher, M., Topping, D.,
 1154 Doughty, D. C., Hill, S. C. and Pan, Y.: Real-time sensing of bioaerosols: Review and current
 1155 perspectives, *Aerosol Sci. Technol.*, 54(5), 465–495, doi:10.1080/02786826.2019.1664724, 2020.

1156 Huneeus, N., Schulz, M., Balkanski, Y., Griesfeller, J., Prospero, J., Kinne, S., Bauer, S., Boucher, O.,
 1157 Chin, M., Dentener, F., Diehl, T., Easter, R., Fillmore, D., Ghan, S., Ginoux, P., Grini, A., Horowitz, L.,
 1158 Koch, D., Krol, M. C., Landing, W., Liu, X., Mahowald, N., Miller, R., Morcrette, J.-J., Myhre, G.,

1159 Penner, J., Perlwitz, J., Stier, P., Takemura, T. and Zender, C. S.: Global dust model intercomparison in
1160 AeroCom phase I, *Atmos. Chem. Phys.*, 11(15), 7781–7816, doi:10.5194/acp-11-7781-2011, 2011.

1161 Kanji, Z. A., Ladino, L. A., Wex, H., Boose, Y., Burkert-Kohn, M., Cziczo, D. J. and Krämer, M.:
1162 Overview of Ice Nucleating Particles, *Meteorol. Monogr.*, 58, 1.1-1.33, doi:10.1175/amsmonographs-d-
1163 16-0006.1, 2017.

1164 Khaniabadi, Y. O., Daryanoosh, S. M., Amrane, A., Polosa, R., Hopke, P. K., Goudarzi, G., Mohammadi,
1165 M. J., Sicard, P. and Armin, H.: Impact of Middle Eastern Dust storms on human health, *Atmos. Pollut.*
1166 *Res.*, 8(4), 606–613, doi:https://doi.org/10.1016/j.apr.2016.11.005, 2017.

1167 Kinne, S., Schulz, M., Textor, C., Guibert, S., Balkanski, Y., Bauer, S. E., Berntsen, T., Berglen, T. F.,
1168 Boucher, O., Chin, M., Collins, W., Dentener, F., Diehl, T., Easter, R., Feichter, J., Fillmore, D., Ghan,
1169 S., Ginoux, P., Gong, S., Grini, A., Hendricks, J., Herzog, M., Horowitz, L., Isaksen, I., Iversen, T.,
1170 Kirkevåg, A., Kloster, S., Koch, D., Kristjansson, J. E., Krol, M., Lauer, A., Lamarque, J. F., Lesins, G.,
1171 Liu, X., Lohmann, U., Montanaro, V., Myhre, G., Penner, J., Pitari, G., Reddy, S., Seland, O., Stier, P.,
1172 Takemura, T. and Tie, X.: An AeroCom initial assessment – optical properties in aerosol component
1173 modules of global models, *Atmos. Chem. Phys.*, 6(7), 1815–1834, doi:10.5194/acp-6-1815-2006, 2006.

1174 Kleist, D. T., Parrish, D. F., Derber, J. C., Treadon, R., Wu, W.-S. and Lord, S.: Introduction of the GSI
1175 into the NCEP Global Data Assimilation System, *Weather Forecast.*, 24(6), 1691–1705,
1176 doi:10.1175/2009WAF2222201.1, 2009.

1177 Klingmüller, K., Pozzer, A., Metzger, S., Stenchikov, G. L. and Lelieveld, J.: Aerosol optical depth trend
1178 over the Middle East, *Atmos. Chem. Phys.*, 16(8), 5063–5073, doi:10.5194/acp-16-5063-2016, 2016.

1179 Knopf, D. A. and Koop, T.: Heterogeneous nucleation of ice on surrogates of mineral dust, *J. Geophys.*
1180 *Res. Atmos.*, 111(D12), doi:https://doi.org/10.1029/2005JD006894, 2006.

1181 Kok, J. F., Adebisi, A. A., Albani, S., Balkanski, Y., Checa-Garcia, R., Chin, M., Colarco, P. R.,
1182 Hamilton, D. S., Huang, Y., Ito, A., Klose, M., Li, L., Mahowald, N. M., Miller, R. L., Obiso, V., Pérez
1183 Garc\'ia-Pando, C., Rocha-Lima, A. and Wan, J. S.: Contribution of the world's main dust source regions
1184 to the global cycle of desert dust, *Atmos. Chem. Phys.*, 21(10), 8169–8193, doi:10.5194/acp-21-8169-
1185 2021, 2021.

1186 Könemann, T., Savage, N., Klimach, T., Walter, D., Fröhlich-Nowoisky, J., Su, H., Pöschl, U., Huffman,
1187 J. A. and Pöhlker, C.: Spectral Intensity Bioaerosol Sensor (SIBS): an instrument for spectrally resolved
1188 fluorescence detection of single particles in real time, *Atmos. Meas. Tech.*, 12(2), 1337–1363,
1189 doi:10.5194/amt-12-1337-2019, 2019.

1190 Krasnov, H., Katra, I. and Friger, M.: Increase in dust storm related PM10 concentrations: A time series
1191 analysis of 2001–2015, *Environ. Pollut.*, 213, 36–42, doi:<https://doi.org/10.1016/j.envpol.2015.10.021>,
1192 2016.

1193 Krueger, B. J., Grassian, V. H., Cowin, J. P. and Laskin, A.: Heterogeneous chemistry of individual
1194 mineral dust particles from different dust source regions: the importance of particle mineralogy, *Atmos.*
1195 *Environ.*, 38(36), 6253–6261, doi:<https://doi.org/10.1016/j.atmosenv.2004.07.010>, 2004.

1196 Krzywinski, M. and Altman, N.: Error bars, *Nat. Methods*, 10(10), 921–922, doi:10.1038/nmeth.2659,
1197 2013.

1198 Ladino, L. A., Raga, G. B., Alvarez-Ospina, H., Andino-Enríquez, M. A., Rosas, I., Martínez, L.,
1199 Salinas, E., Miranda, J., Ramírez-Díaz, Z., Figueroa, B., Chou, C., Bertram, A. K., Quintana, E. T.,
1200 Maldonado, L. A., García-Reynoso, A., Si, M. and Irish, V. E.: Ice-nucleating particles in a coastal
1201 tropical site, *Atmos. Chem. Phys.*, 19(9), 6147–6165, doi:10.5194/acp-19-6147-2019, 2019.

1202 Lohmann, U. and Feichter, J.: Global indirect aerosol effects: a review, *Atmos. Chem. Phys.*, 5(3), 715–
1203 737, doi:10.5194/acp-5-715-2005, 2005.

1204 Manders, A. M. ., Schapp, M., Jozwicka, M., van Arkel, F., Weijers, E. . and Matthijsen, J.: The
1205 contribution of sea salt to PM 10 and PM in the Netherlands, [online] Available from:
1206 <http://www.pbl.nl/sites/default/files/cms/publicaties/500099004.pdf>, 2009.

1207 Martin, A. C., Cornwell, G., Beall, C. M., Cannon, F., Reilly, S., Schaap, B., Lucero, D., Creamean, J.,
1208 Ralph, F. M., Mix, H. T. and Prather, K.: Contrasting local and long-range-transported warm ice-
1209 nucleating particles during an atmospheric river in coastal California, USA, *Atmos. Chem. Phys.*, 19(7),
1210 4193–4210, doi:10.5194/acp-19-4193-2019, 2019.

1211 Mayol, E., Jiménez, M. A., Herndl, G. J., Duarte, C. M. and Arrieta, J. M.: Resolving the abundance and
1212 air-sea fluxes of airborne microorganisms in the North Atlantic Ocean, *Front. Microbiol.*, 5, 557,
1213 doi:10.3389/fmicb.2014.00557, 2014.

1214 McCluskey, C. S., Hill, T. C. J., Malfatti, F., Sultana, C. M., Lee, C., Santander, M. V., Beall, C. M.,
1215 Moore, K. A., Cornwell, G. C., Collins, D. B., Prather, K. A., Jayarathne, T., Stone, E. A., Azam, F.,
1216 Kreidenweis, S. M. and DeMott, P. J.: A Dynamic Link between Ice Nucleating Particles Released in
1217 Nascent Sea Spray Aerosol and Oceanic Biological Activity during Two Mesocosm Experiments, *J.*
1218 *Atmos. Sci.*, 74(1), 151–166, doi:10.1175/JAS-D-16-0087.1, 2017.

1219 McCluskey, C. S., Hill, T. C. J., Sultana, C. M., Laskina, O., Trueblood, J., Santander, M. V., Beall, C.

1220 M., Michaud, J. M., Kreidenweis, S. M., Prather, K. A., Grassian, V., DeMott, P. J., McCluskey, C. S.,
1221 Hill, T. C. J., Sultana, C. M., Laskina, O., Trueblood, J., Santander, M. V., Beall, C. M., Michaud, J. M.,
1222 Kreidenweis, S. M., Prather, K. A., Grassian, V. and DeMott, P. J.: A mesocosm double feature: Insights
1223 into the chemical make-up of marine ice nucleating particles, *J. Atmos. Sci.*, JAS-D-17-0155.1,
1224 doi:10.1175/JAS-D-17-0155.1, 2018a.

1225 McCluskey, C. S., Hill, T. C. J., Sultana, C. M., Laskina, O., Trueblood, J., Santander, M. V., Beall, C.
1226 M., Michaud, J. M., Kreidenweis, S. M., Prather, K. A., Grassian, V. and DeMott, P. J.: A Mesocosm
1227 Double Feature: Insights into the Chemical Makeup of Marine Ice Nucleating Particles, *J. Atmos. Sci.*,
1228 75(7), 2405–2423, doi:10.1175/JAS-D-17-0155.1, 2018b.

1229 McCluskey, C. S., Ovadnevaite, J., Rinaldi, M., Atkinson, J., Belosi, F., Ceburnis, D., Marullo, S., Hill,
1230 T. C. J., Lohmann, U., Kanji, Z. A., O’Dowd, C., Kreidenweis, S. M. and DeMott, P. J.: Marine and
1231 Terrestrial Organic Ice-Nucleating Particles in Pristine Marine to Continentally Influenced Northeast
1232 Atlantic Air Masses, *J. Geophys. Res. Atmos.*, 123(11), 6196–6212, doi:10.1029/2017JD028033, 2018c.

1233 McCluskey, C. S., Hill, T. C. J., Humphries, R. S., Rauker, A. M., Moreau, S., Stratton, P. G., Chambers,
1234 S. D., Williams, A. G. and McRobert, I.: Observations of Ice Nucleating Particles Over Southern Ocean
1235 Waters, *Geophys. Res. Lett.*, 989–997, doi:10.1029/2018GL079981, 2018d.

1236 Mitts, B., Wang, X., Lucero, D., Beall, C., Deane, G., DeMott, P. and Prather, K.: Importance of
1237 Supermicron Ice Nucleating Particles in Nascent Sea Spray, *Geophys. Res. Lett.*, n/a(n/a),
1238 e2020GL089633, doi:https://doi.org/10.1029/2020GL089633, 2021.

1239 Molod, A., Takacs, L., Suarez, M. and Bacmeister, J.: Development of the GEOS-5 atmospheric general
1240 circulation model: evolution from MERRA to MERRA2, *Geosci. Model Dev.*, 8(5), 1339–1356,
1241 doi:10.5194/gmd-8-1339-2015, 2015.

1242 Murray, B. J., O’Sullivan, D., Atkinson, J. D. and Webb, M. E.: Ice nucleation by particles immersed in
1243 supercooled cloud droplets., *Chem. Soc. Rev.*, 41(19), 6519–54, doi:10.1039/c2cs35200a, 2012.

1244 Nickovic, S., Vukovic, A., Vujadinovic, M., Djurdjevic, V. and Pejanovic, G.: Technical Note: High-
1245 resolution mineralogical database of dust-productive soils for atmospheric dust modeling, *Atmos. Chem.*
1246 *Phys.*, 12(2), 845–855, doi:10.5194/acp-12-845-2012, 2012.

1247 Niedermeier, D., Augustin-Bauditz, S., Hartmann, S., Wex, H., Ignatius, K. and Stratmann, F.: Can we
1248 define an asymptotic value for the ice active surface site density for heterogeneous ice nucleation?, *J.*
1249 *Geophys. Res. Atmos.*, 120(10), 5036–5046, doi:https://doi.org/10.1002/2014JD022814, 2015.

1250 Niemand, M., Möhler, O., Vogel, B., Vogel, H., Hoose, C., Connolly, P., Klein, H., Bingemer, H.,
1251 Demott, P., Skrotzki, J. and Leisner, T.: A particle-surface-area-based parameterization of immersion
1252 freezing on desert dust particles, *J. Atmos. Sci.*, 69(10), 3077–3092, doi:10.1175/JAS-D-11-0249.1, 2012.

1253 Nortcliff, S.: *World Soil Resources and Food Security*. Edited by R. Lal and BA Stewart. Boca Raton, FL,
1254 USA: CRC Press (2012), pp. 574,£82.00. ISBN-13: 978-1439844502., *Exp. Agric.*, 48(2), 305–306,
1255 2012.

1256 O’Sullivan, D., Murray, B. J., Malkin, T. L., Whale, T. F., Umo, N. S., Atkinson, J. D., Price, H. C.,
1257 Baustian, K. J., Browse, J. and Webb, M. E.: Ice nucleation by fertile soil dusts: relative importance of
1258 mineral and biogenic components, *Atmos. Chem. Phys.*, 14(4), 1853–1867, doi:10.5194/acp-14-1853-
1259 2014, 2014.

1260 O’Sullivan, D., Adams, M. P., Tarn, M. D., Harrison, A. D., Vergara-Temprado, J., Porter, G. C. E.,
1261 Holden, M. A., Sanchez-Marroquin, A., Carotenuto, F., Whale, T. F., McQuaid, J. B., Walshaw, R.,
1262 Hedges, D. H. P., Burke, I. T., Cui, Z. and Murray, B. J.: Contributions of biogenic material to the
1263 atmospheric ice-nucleating particle population in North Western Europe, *Sci. Rep.*, 8(1), 13821,
1264 doi:10.1038/s41598-018-31981-7, 2018.

1265 Paramonov, M., David, R. O., Kretschmar, R. and Kanji, Z. A.: A laboratory investigation of the ice
1266 nucleation efficiency of three types of mineral and soil dust, *Atmos. Chem. Phys.*, 18(22), 16515–16536,
1267 doi:10.5194/acp-18-16515-2018, 2018.

1268 Van Pelt, R. S. and Zobeck, T. M.: Chemical Constituents of Fugitive Dust, *Environ. Monit. Assess.*,
1269 130(1), 3–16, doi:10.1007/s10661-006-9446-8, 2007.

1270 Perkins, R. J., Gillette, S. M., Hill, T. C. J. and DeMott, P. J.: The Labile Nature of Ice Nucleation by
1271 Arizona Test Dust, *ACS Earth Sp. Chem.*, 4(1), 133–141, doi:10.1021/acsearthspacechem.9b00304,
1272 2020.

1273 Pfannerstill, E. Y., Wang, N., Edtbauer, A., Bourtsoukidis, E., Crowley, J. N., Dienhart, D., Eger, P. G.,
1274 Ernle, L., Fischer, H., Hottmann, B., Paris, J.-D., Stöner, C., Tadic, I., Walter, D., Lelieveld, J. and
1275 Williams, J.: Shipborne measurements of total OH reactivity around the Arabian Peninsula and its role in
1276 ozone chemistry, *Atmos. Chem. Phys.*, 19(17), 11501–11523, doi:10.5194/acp-19-11501-2019, 2019.

1277 Price, H. C., Baustian, K. J., McQuaid, J. B., Blyth, A., Bower, K. N., Choularton, T., Cotton, R. J., Cui,
1278 Z., Field, P. R., Gallagher, M., Hawker, R., Merrington, A., Miltenberger, A., Neely III, R. R., Parker, S.
1279 T., Rosenberg, P. D., Taylor, J. W., Trembath, J., Vergara-Temprado, J., Whale, T. F., Wilson, T. W.,
1280 Young, G. and Murray, B. J.: Atmospheric Ice-Nucleating Particles in the Dusty Tropical Atlantic, *J.*

1281 Geophys. Res. Atmos., 123(4), 2175–2193, doi:<https://doi.org/10.1002/2017JD027560>, 2018.

1282 Prodi, F., Santachiara, G. and Oliosì, F.: Characterization of aerosols in marine environments
1283 (Mediterranean, Red Sea, and Indian Ocean), *J. Geophys. Res. Ocean.*, 88(C15), 10957–10968,
1284 doi:<https://doi.org/10.1029/JC088iC15p10957>, 1983.

1285 Rienecker, M. M., Suarez, M. J., Gelaro, R., Todling, R., Bacmeister, J., Liu, E., Bosilovich, M. G.,
1286 Schubert, S. D., Takacs, L., Kim, G.-K., Bloom, S., Chen, J., Collins, D., Conaty, A., da Silva, A., Gu,
1287 W., Joiner, J., Koster, R. D., Lucchesi, R., Molod, A., Owens, T., Pawson, S., Pegion, P., Redder, C. R.,
1288 Reichle, R., Robertson, F. R., Ruddick, A. G., Sienkiewicz, M. and Woollen, J.: MERRA: NASA's
1289 Modern-Era Retrospective Analysis for Research and Applications, *J. Clim.*, 24(14), 3624–3648,
1290 doi:10.1175/JCLI-D-11-00015.1, 2011.

1291 Salam, A., Lohmann, U. and Lesins, G.: Ice nucleation of ammonia gas exposed montmorillonite mineral
1292 dust particles, *Atmos. Chem. Phys.*, 7(14), 3923–3931, doi:10.5194/acp-7-3923-2007, 2007.

1293 Schnell, R. C.: Ice Nuclei in Seawater, Fog Water and Marine Air off the Coast of Nova Scotia: Summer
1294 1975, *J. Atmos. Sci.*, 34(8), 1299–1305, doi:10.1175/1520-0469(1977)034<1299:INISFW>2.0.CO;2,
1295 1977.

1296 Schrod, J., Weber, D., Drücke, J., Keleshis, C., Pikridas, M., Ebert, M., Cvetković, B., Nickovic, S.,
1297 Marinou, E., Baars, H., Ansmann, A., Vrekoussis, M., Mihalopoulos, N., Sciare, J., Curtius, J. and
1298 Bingemer, H. G.: Ice nucleating particles over the Eastern Mediterranean measured by unmanned aircraft
1299 systems, *Atmos. Chem. Phys.*, 17(7), 4817–4835, doi:10.5194/acp-17-4817-2017, 2017.

1300 Shahsavani, A., Naddafī, K., Jafarzade Haghhighifard, N., Mesdaghinia, A., Yunesian, M., Nabizadeh, R.,
1301 Arahani, M., Sowlat, M. H., Yarahmadi, M., Saki, H., Alimohamadi, M., Nazmara, S., Motevalian, S. A.
1302 and Goudarzi, G.: The evaluation of PM₁₀, PM_{2.5}, and PM₁ concentrations during the Middle Eastern
1303 Dust (MED) events in Ahvaz, Iran, from april through september 2010, *J. Arid Environ.*, 77, 72–83,
1304 doi:<https://doi.org/10.1016/j.jaridenv.2011.09.007>, 2012.

1305 Sullivan, R. C., Guazzotti, S. A., Sodeman, D. A. and Prather, K. A.: Direct observations of the
1306 atmospheric processing of Asian mineral dust, *Atmos. Chem. Phys.*, 7(5), 1213–1236, doi:10.5194/acp-7-
1307 1213-2007, 2007.

1308 Sullivan, R. C., Miñambres, L., DeMott, P. J., Prenni, A. J., Carrico, C. M., Levin, E. J. T. and
1309 Kreidenweis, S. M.: Chemical processing does not always impair heterogeneous ice nucleation of mineral
1310 dust particles, *Geophys. Res. Lett.*, 37(24), doi:<https://doi.org/10.1029/2010GL045540>, 2010a.

1311 Sullivan, R. C., Petters, M. D., DeMott, P. J., Kreidenweis, S. M., Wex, H., Niedermeier, D., Hartmann,
1312 S., Clauss, T., Stratmann, F., Reitz, P., Schneider, J. and Sierau, B.: Irreversible loss of ice nucleation
1313 active sites in mineral dust particles caused by sulphuric acid condensation, *Atmos. Chem. Phys.*, 10(23),
1314 11471–11487, doi:10.5194/acp-10-11471-2010, 2010b.

1315 Suski, K. J., Hill, T. C. J., Levin, E. J. T., Miller, A., DeMott, P. J. and Kreidenweis, S. M.: Agricultural
1316 harvesting emissions of ice-nucleating particles, *Atmos. Chem. Phys.*, 18(18), 13755–13771,
1317 doi:10.5194/acp-18-13755-2018, 2018.

1318 Tadic, I., Crowley, J. N., Dienhart, D., Eger, P., Harder, H., Hottmann, B., Martinez, M., Parchatka, U.,
1319 Paris, J.-D., Pozzer, A., Rohloff, R., Schuladen, J., Shenolikar, J., Tauer, S., Lelieveld, J. and Fischer, H.:
1320 Net ozone production and its relationship to nitrogen oxides and volatile organic compounds in the
1321 marine boundary layer around the Arabian Peninsula, *Atmos. Chem. Phys.*, 20(11), 6769–6787,
1322 doi:10.5194/acp-20-6769-2020, 2020.

1323 Tobo, Y., DeMott, P. J., Hill, T. C. J., Prenni, A. J., Swoboda-Colberg, N. G., Franc, G. D. and
1324 Kreidenweis, S. M.: Organic matter matters for ice nuclei of agricultural soil origin, *Atmos. Chem. Phys.*,
1325 14(16), 8521–8531, doi:10.5194/acp-14-8521-2014, 2014.

1326 Ullrich, R., Hoose, C., Möhler, O., Niemand, M., Wagner, R., Höhler, K., Hiranuma, N., Saathoff, H. and
1327 Leisner, T.: A new ice nucleation active site parameterization for desert dust and soot, *J. Atmos. Sci.*,
1328 74(3), 699–717, doi:10.1175/JAS-D-16-0074.1, 2017.

1329 Vali, G.: Quantitative Evaluation of Experimental Results on the Heterogeneous Freezing Nucleation of
1330 Supercooled Liquids, *J. Atmos. Sci.*, 28(3), 402–409, doi:10.1175/1520-
1331 0469(1971)028<0402:QEOERA>2.0.CO;2, 1971.

1332 Vergara-Temprado, J., Murray, B. J., Wilson, T. W., O’Sullivan, D., Browse, J., Pringle, K. J., Ardon-
1333 Dryer, K., Bertram, A. K., Burrows, S. M., Ceburnis, D., Demott, P. J., Mason, R. H., O’Dowd, C. D.,
1334 Rinaldi, M. and Carslaw, K. S.: Contribution of feldspar and marine organic aerosols to global ice
1335 nucleating particle concentrations, *Atmos. Chem. Phys.*, 17(5), 3637–3658, doi:10.5194/acp-17-3637-
1336 2017, 2017.

1337 Vergara-Temprado, J., Miltenberger, A. K., Furtado, K., Grosvenor, D. P., Shipway, B. J., Hill, A. A.,
1338 Wilkinson, J. M., Field, P. R., Murray, B. J. and Carslaw, K. S.: Strong control of Southern Ocean cloud
1339 reflectivity by ice-nucleating particles, *Proc. Natl. Acad. Sci.*, 115(11), 2687 LP – 2692,
1340 doi:10.1073/pnas.1721627115, 2018.

1341 Wang, N., Edtbauer, A., Stöner, C., Pozzer, A., Bourtsoukidis, E., Ernle, L., Dienhart, D., Hottmann, B.,

1342 Fischer, H., Schuladen, J., Crowley, J. N., Paris, J.-D., Lelieveld, J. and Williams, J.: Measurements of
1343 carbonyl compounds around the Arabian Peninsula: overview and model comparison, *Atmos. Chem.*
1344 *Phys.*, 20(18), 10807–10829, doi:10.5194/acp-20-10807-2020, 2020.

1345 Wang, X., Deane, G. B., Moore, K. A., Ryder, O. S., Stokes, M. D., Beall, C. M., Collins, D. B.,
1346 Santander, M. V., Burrows, S. M., Sultana, C. M. and Prather, K. A.: The role of jet and film drops in
1347 controlling the mixing state of submicron sea spray aerosol particles, *Proc. Natl. Acad. Sci.*, 114(27),
1348 6978–6983, doi:10.1073/pnas.1702420114, 2017.

1349 von der Weiden, S.-L., Drewnick, F. and Borrmann, S.: Particle Loss Calculator – a new software tool for
1350 the assessment of the performance of aerosol inlet systems, *Atmos. Meas. Tech.*, 2(2), 479–494,
1351 doi:10.5194/amt-2-479-2009, 2009.

1352 Welti, A., Lüönd, F., Kanji, Z. A., Stetzer, O. and Lohmann, U.: Time dependence of immersion freezing:
1353 an experimental study on size selected kaolinite particles, *Atmos. Chem. Phys.*, 12(20), 9893–9907,
1354 doi:10.5194/acp-12-9893-2012, 2012.

1355 Wex, H., DeMott, P. J., Tobo, Y., Hartmann, S., Rösch, M., Clauss, T., Tomsche, L., Niedermeier, D. and
1356 Stratmann, F.: Kaolinite particles as ice nuclei: learning from the use of different kaolinite samples and
1357 different coatings, *Atmos. Chem. Phys.*, 14(11), 5529–5546, doi:10.5194/acp-14-5529-2014, 2014.

1358 Wex, H., Huang, L., Zhang, W., Hung, H., Traversi, R., Becagli, S., Sheesley, R. J., Moffett, C. E.,
1359 Barrett, T. E., Bossi, R., Skov, H., Hünerbein, A., Lubitz, J., Löffler, M., Linke, O., Hartmann, M.,
1360 Herenz, P. and Stratmann, F.: Annual variability of ice-nucleating particle concentrations at different
1361 Arctic locations, *Atmos. Chem. Phys.*, 19(7), 5293–5311, doi:10.5194/acp-19-5293-2019, 2019.

1362 Whale, T. F., Murray, B. J., O’Sullivan, D., Wilson, T. W., Umo, N. S., Baustian, K. J., Atkinson, J. D.,
1363 Workneh, D. A. and Morris, G. J.: A technique for quantifying heterogeneous ice nucleation in microlitre
1364 supercooled water droplets, *Atmos. Meas. Tech.*, 8(6), 2437–2447, doi:10.5194/amt-8-2437-2015, 2015.

1365 Wilson, T. W., Ladino, L. a., Alpert, P. a., Breckels, M. N., Brooks, I. M., Browse, J., Burrows, S. M.,
1366 Carslaw, K. S., Huffman, J. A., Judd, C., Kilhau, W. P., Mason, R. H., McFiggans, G., Miller, L. a.,
1367 Nájera, J. J., Polishchuk, E., Rae, S., Schiller, C. L., Si, M., Temprado, J. V., Whale, T. F., Wong, J. P. S.,
1368 Wurl, O., Yakobi-Hancock, J. D., Abbatt, J. P. D., Aller, J. Y., Bertram, A. K., Knopf, D. a. and Murray,
1369 B. J.: A marine biogenic source of atmospheric ice-nucleating particles, *Nature*, 525(7568), 234–238,
1370 doi:10.1038/nature14986, 2015.

1371 Wu, W.-S., Purser, R. J. and Parish, D. F.: Three-Dimensional Variational Analysis with Spatially
1372 Inhomogeneous Covariances, *Mon. Weather Rev.*, 130(12), 2905–2916, doi:10.1175/1520-

1373 0493(2002)130<2905:TDVAWS>2.0.CO;2, 2002.

1374 Yadav, S., Venezia, R. E., Paerl, R. W. and Petters, M. D.: Characterization of Ice-Nucleating Particles
1375 Over Northern India, *J. Geophys. Res. Atmos.*, 124(19), 10467–10482,
1376 doi:<https://doi.org/10.1029/2019JD030702>, 2019.

1377 Yahya, R. Z., Arrieta, J. M., Cusack, M. and Duarte, C. M.: Airborne Prokaryote and Virus Abundance
1378 Over the Red Sea, *Front. Microbiol.*, 10, 1112, doi:10.3389/fmicb.2019.01112, 2019.

1379 Yang, J., Wang, Z., Heymsfield, A. J., DeMott, P. J., Twohy, C. H., Suski, K. J. and Toohey, D. W.: High
1380 ice concentration observed in tropical maritime stratiform mixed-phase clouds with top temperatures
1381 warmer than -8°C , *Atmos. Res.*, 233, 104719, doi:<https://doi.org/10.1016/j.atmosres.2019.104719>, 2020.

1382 Yost, J. L. and Hartemink, A. E.: Chapter Four - Soil organic carbon in sandy soils: A review, vol. 158,
1383 edited by D. L. Sparks, pp. 217–310, Academic Press., 2019.

1384 Yu, Y., Kalashnikova, O. V., Garay, M. J., Lee, H. and Notaro, M.: Identification and Characterization of
1385 Dust Source Regions Across North Africa and the Middle East Using MISR Satellite Observations,
1386 *Geophys. Res. Lett.*, 45(13), 6690–6701, doi:<https://doi.org/10.1029/2018GL078324>, 2018.

1387 Zolles, T., Burkart, J., Häusler, T., Pummer, B., Hitznerberger, R. and Grothe, H.: Identification of Ice
1388 Nucleation Active Sites on Feldspar Dust Particles, *J. Phys. Chem. A*, 119(11), 2692–2700,
1389 doi:10.1021/jp509839x, 2015.

1390